APPLICATIONS OF MAGNETIC HYPERTHERMIA USING MAGNETIC NANOPARTICLES CONJUGATED WITH SPECIFIC DNA PARTICULATES

by
Kemal Düzkar

Submitted to Graduate School of Natural and Applied Sciences
in Partial Fulfillment of the Requirements
for the Degree of Master of Science in
Chemical Engineering

Yeditepe University
2022

APPLICATIONS OF MAGNETIC HYPERTHERMIA USING MAGNETIC NANOPARTICLES CONJUGATED WITH SPECIFIC DNA PARTICULATES

APPROVED BY:

Assist. Prof. Dr. Cem Levent Altan ……
(Thesis Supervisor)
(Yeditepe University)

Prof. Dr. Amitav Sanyal ……
(Bogazici University)

Assist. Prof. Dr. Mehmet Hikmet Üçışık ……
(Yeditepe University)

DATE OF APPROVAL: …./…./2022

I hereby declare that this thesis is my own work and that all information in this thesis has been obtained and presented in accordance with academic rules and ethical conduct. I have fully cited and referenced all material and results as required by these rules and conduct, and this thesis study does not contain any plagiarism. If any material used in the thesis requires copyright, the necessary permissions have been obtained. No material from this thesis has been used for the award of another degree.

I accept all kinds of legal liability that may arise in case contrary to these situations.

Name, Last name Kemal Düzkar

Signature …..……..……..

ACKNOWLEDGEMENTS

First of all, I would like to express my special gratitude to my supervisor Assist. Prof. Dr. Cem Levent Altan. Being by my side with his inexhaustible energy and patience since the first day we met, he has made me a visionary not only in academia, but also in all parts of life. I feel extremely lucky to be working with such a valuable scientist and great person. Also, I would like to thank Melis Çağdaş for her valuable perspective and feedbacks.

I would also like to thank Mehmet H. Ucisik, Sibel S. Erdem, Gizem Keceloglu and Irem Gorali for their contributions in this project.

I am grateful to all of those with whom I have had the pleasure to work during graduate years. Particularly, I would like to thank Beyza Abişoğlu, Berk S. Alarcin, and Ezgi Uslu for the wonderful times we shared, and supporting me through this entire process. This journey would truly meaningless without them. I also offer my gratitude to all my other colleagues.

Also, I would like to thank my beloved family who have dedicated their lives to providing me with all these opportunities. Thank you for always being there for me and making me feel their love and support.

Lastly, I would like to thank my inner voice, which allows me to push the boundaries whenever I encountered with challenges.

ABSTRACT

APPLICATIONS OF MAGNETIC HYPERTHERMIA USING MAGNETIC NANOPARTICLES CONJUGATED WITH SPECIFIC DNA PARTICULATES

In recent years, the inadequacy of conventional treatment methods for cancer considerably arises the interest in complementary and alternative approaches. Hyperthermia is the local heating of tumor site results in the destruction of cancer cells either by a programmable or premature death of malignant cells without affecting healthy cells In magnetic hyperthermia, the targeting and uniform distribution of magnetic nanoparticles to the tumor site is cruical for improving the efficiency of the treatment method. In this study, magnetite nanoparticles that are functionalized with PAA were synthesized via aqueous partial oxidation method. Furthermore, these magnetic particles were conjugated with a DNA sequence (DeNAno), which identify and bind to pancreatic cancer cell lines for possible magnetic hyperthermia applications. By applying alternating magnetic field, the specific absorption rate (SAR) of PAA functionalized ferrimagnetic nanoparticles has been studied as a function of magnetic field strength, frequency and particle concentration. The results indicated that the heating performance of ferrimagnetic nanoparticles and consequently the SAR enhanced with increasing magnetic field intensities and frequencies. Moreover, the variation of the molecular weight of polymer, that is attached onto surface of nanoparticles was shown to affect the corresponding SAR value. Furthermore, a significant decrease in the SAR of ferrimagnetic magnetite nanoparticles by increasing particle loading were observed. These bahaviours were attributed to the interparticle dipole-dipole interaction that increases at higher particle concentrations which may lower the hyperthermia efficiency of the particles and decrease the SAR. The results further shown that, DeNAno particulates which are synthesized via RCA process were successfully conjugated with magnetic nanoparticles that exhibit significant saturation magnetizaton and the entity still maintain its target specific binding characteristics and adversely affect cancer cell viability all of which consequently indicate their potential application in magnetic hyperthermia as a active targeting system.

This work was supported by the Scientific and Technological Research Council of Turkey (TÜBİTAK), Project Nr.216Z004.

ÖZET

ÖZEL DNA PARTİKÜLLERİ İLE KONJUGE EDİLMİŞ MANYETİK NANOPARÇACIKLARIN MANYETİK HİPERTERMİ UYGULAMALARI

Kanser için geleneksel tedavi yöntemlerinin yetersizliği tamamlayıcı ve alternatif yaklaşımlara olan ilgiyi önemli ölçüde artırmaktadır. Hipertermi vücut sıcaklığından yüksek değerlere lokal olarak ulaşılarak sağlıklı hücrelere etki etmeden kanser hücrelerine zarar verilmesi veya tamamen ortadan kaldırılması için kullanılan alternatif bir terapi yöntemidir. Manyetik hipertermi uygulamalarında manyetik nanoparçacıkların tümörlü bölgeye hedeflendirilmesi ve dağılımlarının sağlanması, verimliliklerinin arttırılması adına önem taşımaktadır. Bu çalışmada, yüzeyleri PAA ile modifiye edilmiş magnetit nanoparçacıkları kısmi oksitlenme yöntemi ile sentezlenmiş ve pankreas kanser hücre hattına seçiciliği önceden gösterilmiş bir DNA dizisi (DeNAno) ile hipertermi uygulamalarında kullanılması mümkün olan bir konjugat haline getirilmiştir. Alternatif bir manyetik alan altında PAA ile fonksiyonlandırılmış ferrimanyetik nanopartiküllerin spesifik absorpsiyon hızları (SAR), uygulanan manyetik alanın şiddetine, frekansına ve parçacık konsantrasyonuna bağlı olarak araştırılmıştır. Sonuçlar, ferrimanyetik nanoparçacıkların hipertermi performansının ve SAR değerlerinin artan manyetik alan şiddeti ve frekansı ile artış gösterdiğini göstermiştir. Ayrıca, SAR değerinin nanoparçacıkların yüzeyinde bulunan polimerin, molekül ağırlığının değişmesi ile farklılık gösterebileceği sunulmuştur. Ek olarak, SAR değerinde nanopartikül konsantrasyonunun arttırılması ile birlikte düşüş gözlemlenmiştir. Bu davranış biçimi, hipertermi verimliliğinin ve SAR değerinin ciddi bir şekilde azalmasına yol açan parçacıklar arası dipol-dipol etkileşiminin yüksek parçacık konsantrasyonlarında artış göstermesine atfedilmiştir. Sonuçlar, RCA yöntemi ile hazırlanan DeNAno nanoparçacıklarının yüksek doygunluk manyetizmasına sahip magnetit nanoparçacıkları ile etkileşime geçebildiklerini, bu etkileşim ve konjugasyon sonucunda hedefe seçicilik özelliklerinin korunduğunu ve kanser hücrelerinin canlılığı üzerinde olumsuz yönde etkide bulunarak aktif hücre hedefleme sistemi olarak hipertermi uygulamalarında kullanılabilme potansiyellerini de ortaya koymuştur. Bu çalışma, Türkiye Bilimsel ve Teknolojik Araştırma Kurumu (Proje No.216Z004) tarafından desteklenmiştir.

TABLE OF CONTENTS

LIST OF FIGURES

LIST OF TABLES

LIST OF SYMBOLS/ABBREVIATIONS

φ	Concentration
°C	Degrees centigrade
ρ	Density
f	Frequency
kA	Kiloamper
kHz	Kilohertz
H_0	Magnetic field amplitude
mAbs	Monoclonal antibodies
mL	Milliliter
C_p	Specific heat capacity

ABS	Absorbance
AMF	Alternating magnetic field
AC	Alternating current
DF	Dilution factor
DLS	Dynamic light scattering
DNA	Deoxyribonucleic acid
DOX	Doxorubicin
EPR	Enhanced permeability and petention
FCC	Face-centered cubic
Fe_3O_4	Magnetite
MNP	Magnetic nanoparticle
MRI	Magnetic resonance imaging
mV	Millivolt
nm	Nanometer
PAA	Polyacrylic acid
PCR	Polymerase chain reaction
PEG	Polyethylene glycol
RCA	Rolling circle amplification
RNA	Ribonucleic acid

RPM	Revolutions per minute
SAED	Selected area electron diffraction
SAR	Specific absorption rate
TEM	Transmission electron microscopy
TGA	Thermogravimetric analysis
TIL	Tumor-infiltrating lymphocyte
UV-Vis	Ultraviolet visible
VSM	Vibrating sample magnetometer
XRD	X-ray diffraction

1. INTRODUCTION

Cancer is a large number of diseases where abnormal cells grow uncontrollably and spread to other organs. Cancer is the second leading cause of death, which is estimated that there will be 27.5 million new cancer cases worldwide each year by 2040 [1]. Even though notable progress has been made in cancer therapy, various types are still untreatable by conventional therapies such as chemotherapy, radiation therapy or surgery. All of these conventional methods for cancer treatment possess several side effects and performed at tissue and organ size scales, however killing and controlling tumors at cellular level is significant. To overcome these limitations, more localized treatment methods are aimed to be developed by considering target specific agents that can diagnose and selectively attach to tumor cells as well as unaffecting the healthy counterparts [2].

Hyperthermia is a term refers to a therapeutic method for cancer treatment using thermal energy focused on cancer cells with minor side effects to surroundings healthy tissues. In hyperthermia treatment, tumor cells are destroyed with the local increment in the temperature of a region to 40-45 ^{o}C, which causes to complete or partial killing by metabolic events including programmable (apoptosis) or premature death (necrosis) of malignant cells.. Magnetic hyperthermia is a branch of hyperthermia which is applied via biocompatible magnetic nanoparticles (MNPs) as heating sources. The ability of heating under alternating magnetic field are defined by specific absorption rate (SAR) which is the rate of heat generation per unit mass of the corresponding magnetic particles [3]. Although the hyperthermia efficiency of superparamagnetic nanoparticles has been extensively investigated in the literature [4–10], studies on hyperthermia related performance of ferrimagnetic nanoparticles are very few due to complicated colloidal stabilization.

For the application of magnetic hyperthermia, magnetic nanoparticles can be delivered into the cancer cells either by injected directly, or targeted by active agents that have specific affinity to the tumor cells. As summarized by numerous studies [3,11,12], the direct injection approach is not suitable due to the necessity of high concentration of magnetic nanoparticles which further lead to systemic toxicity to normal cells. Active

targeting, on the other hand, may results in uniform and homogeneous distribution at the tumor site due to the existence of specific ligands having affinity to cancer cells, thus, relatively lower concentrations of magnetic nanoparticles are neded [3,13–15]. As a consequence, innovative approaches are needed for delivering magnetic nanoparticles to tumor sites and attain uniform distribution to avoid unfavorable concentrations, as well as to enhance the efficiency of hyperthermia treatment.

DeNAno nanoparticles are synthetic affinity reagents that present concetemeric sequence consist of highly condensed DNA nanoparticulates, and have the ability to act as a ligand to specific molecules. DeNAno, unlike its alternatives, connects to its target via interaction of several active molecules having morphology and surface recognition characteristics, rather than through one-to-one molecular interactions. Moreover, DeNAno is synthesized by using random DNA libraries which offer the multivalent binding nature such that DeNAno can be uniformly distributed within the tumor site and act as a ligand to its specific targets [16,17].

In this project, ferrimagnetic nanoparticles functionalized with PAA are synthesized via partial oxidation method and these nanoparticles are conjugated with DeNAno particulates that have the ability of selectively identify and bind to pancreatic cancer cell lines. The hyperthermia performance of both bare and surface modified ferrimagnetic magnetite nanoparticles are measured in terms of specific absorption rate (SAR) as a function of particle concentration, magnetic field strength and frequency. Moreover, the hyperthermia performance of magnetite conjugated DeNAno particulates are tested with pancreatic cancer cell lines. These results will not only contribute to the recent developments in hyperthermia applications for cancer treatment but also bring a novel prespective for some of the essential problems associated with it such as non-uniform distribution of magnetic nanoparticles at the tumor site.

2. THEORETICAL BACKGROUND

2.1. CANCER

2.1.1. Introduction to Cancer

Normally, trillions of human cells grow and multiply over lifetime to form new cells as needed. In the case of cells become damaged or harmed, they usually die and new cells are formed. Cancer starts when this ordinary process evolves into uncontrolled manner by which abnormal cells can grow, multiply and spread into nearby tissues, which further may lead to form tumors, that can be categorized as cancerous (malignant) or non-cancerous (benign) cells. Cancerous tumors can grow and invade into neighbouring tissues and also travel to different locations within the body leading to the formation of tumors via a process called metastasis. On the other hand, a benign tumors can also grow but do not spread into nearby tissues. It should be noted that, benign tumors generally do not regrow when they are removed, whereas cancerous tumors often do. Differences between normal cells and cancerous cells can be seen in Figure 2.1 [1,2].

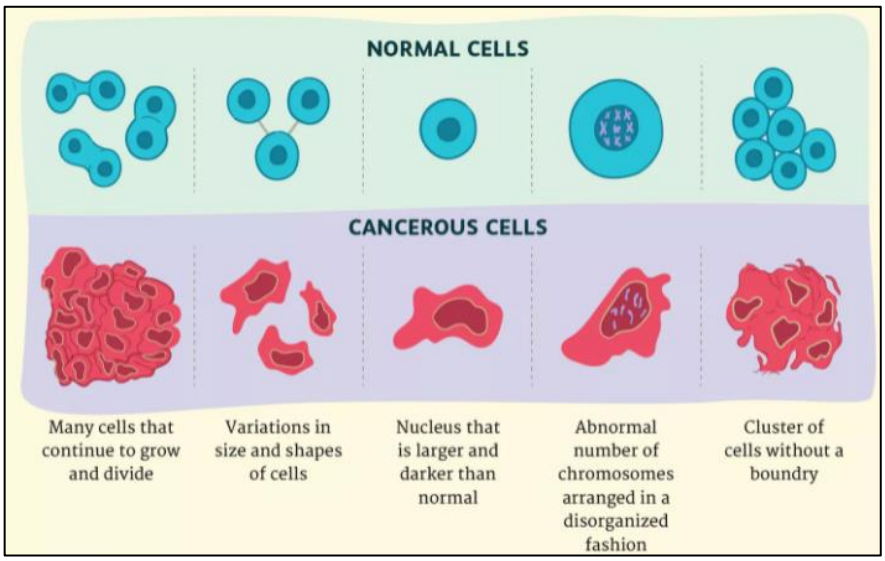

Figure 2.1. Differences between human cells and cancerous cells [18]

It is necessary to understand the fundamental differences between cancer cells and normal cells in order to formulate treatment pathways that aim to destroy cancer cells without harming healthy counterparts. For instance, normal cells stop reproducing and growing when they receive a signal through a process called apoptosis which is briefly the programmed cell death in the presence of sufficient cell amounts. In contrast, cancer cells ignore those signals and keep growing which leads to the formation of cluster of cancer cells namely tumors. Furthermore, normal cells retain their location within the body whereas cancer cells may spread into indistinct tissues or organs through bloodstream and lymphatic system. Normally, the immune system identifies and removes damaged or abnormal cells. On the other hand, cancer cells have the ability to bypass the immune system by releasing chemicals which deactive immune cells [18].

2.1.2. Conventional Treatment Methods

Even though, countless studies have been conducted for efficient cancer treatment methods in recent years, cancer cells can evolve and progress over time that results in new mutations, making cancer treatment even more challenging. Mainly, there are three conventional methods for cancer treatment: chemotherapy, radiotherapy and surgery.

Chemotherapy is a drug based treatment which utilizes cytotoxic chemicals to destroy growing cancerous cells. Chemotherapeutic drugs target cells that have a high basal level of regeneration and proliferation. However, the toxicity associated with chemo drugs also severely affect normal tissues surrounding the tumor. Moreover, since high dosage of drugs are required for broad distribution and fast destruction, economical and toxicity issues need to be considered. There are also controversial studies which revealed scientific proofs for the fact that chemotherapy do not possibly prolong patient's life considerably. [19,20] .

Radiation therapy is another most commonly applied treatment method by the utilization of ionizing radiation to dominate abnormal cell growth or suppress tumoral tissues. Generally, radiotherapy is applied to treat tumors by the ultimate aim of damaging the genetic structure of cancer cells. Unfortunately, this curative effect also damages the healthy tissues surrounding the tumors, which significantly limits the efficiancy and

application of treatment. Conventional radiotherapy can also cause secondary tumors, which depends on factors such as the extent of tumor, patient's age and also the radiation dosage [21].

Surgery is the most traditinonal treatment method by which the tumor is completely taken out from the region of interest generally after the chemo and radiation theraphies which solely or in combination shrink the tumor before the process. It is accepted that surgery also carries risks such as circulation of cancer cells in the bloodstream, infections, and the suppression of immune system. Circulating tumor cells in the blood and reduced immune reactivity as a consequence of operations are regarded as causes of metastases [8,9]. Numerous number of clinical investigations reported that surgery treatment increases the metastases by stimulating the hematogenic dispersion of tumor cells [22].

Since none of these conventional therapies offer effective and ultimate treatment for cancer, synergetic or combination theraphies that merges two or more methods are also applied for several cancer types which may deteriorate or inhibit the toxic effects on healthy cells. In addition, combination treatments increase the chance of killing all cancer cells by targeting the heterogeneous nature of tumors by using multiple perspectives [11]. However, it should be noted that, the expensive combination of multiple theraphies can also produce undesirable collective side-effects associated with considered treatment methods [23,24].

2.1.3. Novel Approaches

The unsatisfactory results of traditional treatments and their toxicity to healthy tissues along with tumor cells have led to the development of new treatment methods for cancer. All of these conventinal methods for cancer treatment is executed at tissue and organ size scales, however killing and controlling tumors at cellular level is critical. To overcome these limitations, novel approaches have emerged to treat cancer more efficiently and complement current conventional therapies. In addition, more localized treatment methods should be developed by considering specific targets, markers or ligands that can be able to identify, recognise and attach to tumor cells selectively.

2.1.3.1. Immunotherapy

For the last decade, immunotherapy has attracted attention as an encouraging therapeutic approach by aiming to use antitumoral effect of immune system affect to tumor cells both therapeutically and prophylactically. In other words, immunotherapy can be described as a class of biotherapy which relies on the immune system sensitization that reduces side effects associated with conventional treatments and increases the selectivity [25].

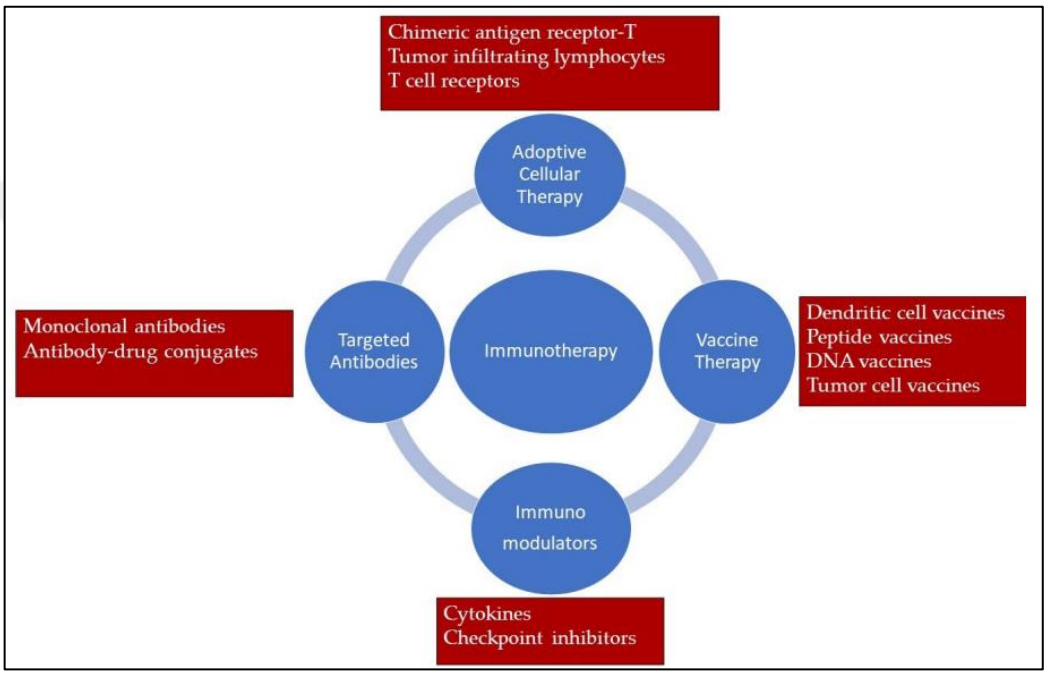

Figure 2.2. Different approches of immunotherapy for cancer treatment [26]

The immune system is a complex network of biological processes, that is made up of different cells, organs and proteins, aiming to detect, respond and distinguish the pathogens, bacteria, viruses and as well as well as cancer cells from the organism's healthy tissue. The immune system attempts to classify the cancer cells by recognizing particular molecules that are uniquely present and named as tumor associated antigents [27]. Even though the immune system recognizes cancer cells and inhibits cancer growth, the cells exert immunosuppression mechanisms which delay tumor from being detected by changing their genetic nature which make them invisible to the immune system [26].

Basically, immonotherapy is categorized into four types as shown in Figure 2.2, which are immunomodulation, adoptive cellular therapy, targeted antibodies and cancer

vaccines. For the application of immunomodulation, the host immune system is activated in order to improve the immune response by the stimulation of antigen cells through T cells, which attact tumor cells. Another immunomodulater group utilized in treatment is checkpoint inhibitors, which block the proteins that are responsible for preventing the immune system from affecting cancer cells [26].

Figure 2.3 represents the adoptive cell transfer, which is the Tumor-Infiltrating Lymphocyte (TIL) therapy is used to improve the operation of naturally occurring T cells that are responsible to extinguish cancer cells. T cells are harvested from the patient, activated, expanded, and given back to the patient. In the case of sufficient T cells are present, tumor cells are aimed to be destroyed [28].

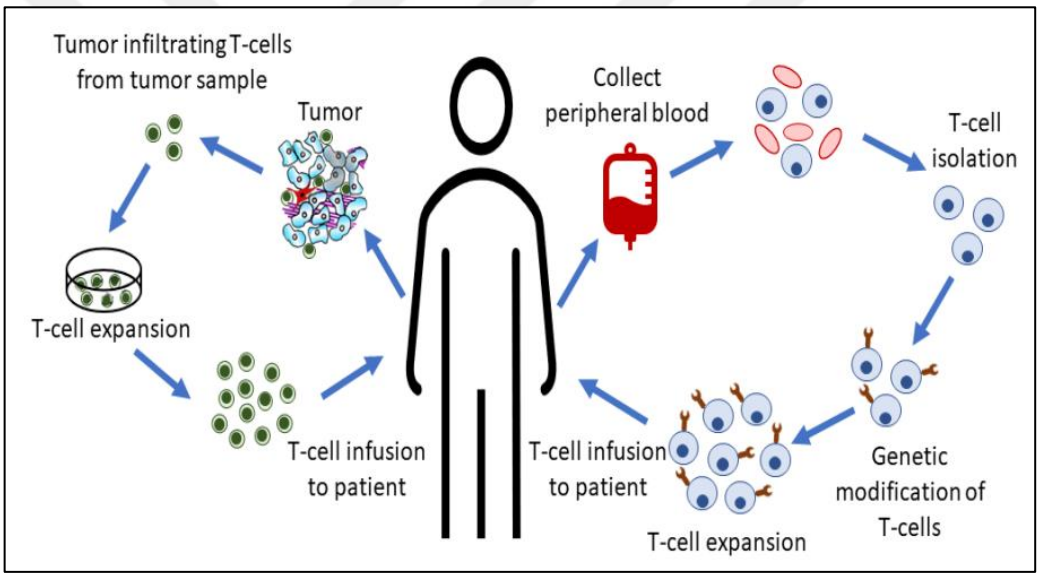

Figure 2.3. Cell therapy approaches [26]

The idea of active targeting in the treatment of cancer disease has led to utilize Monoclonal antibodies (mAbs), which is described as antibodies that can attach to unique parts of an antigen. mAbs are widely applied in cancer treatment along with anticancer agents due to their highly specific binding characteristics which aids to target anticancer drugs to tumor site [29].

Finally, vaccine therapy aims to activate and stimulate the effector functions of the immune system by using antigens or tumor cells in order to destroy the cancer cells and prevent relapse [26].

2.1.3.2. Gene Therapy

The development of Genome engineering has paved the way for gene therapy for the management and prevention of cancer by modifying the DNA codes and altering RNA via post transcriptional modifications. Researchers are optimistic about providing effective approach to patients suffering from single-gene and complex acquired disorders. Gene therapy is based on a correction of a genetic defect by replacing functional, healthy variant of corresponding gene. Gene therapy is a potentially beneficial cancer treatment approach and overcomes the limitations associated with the conventional treatments such as low bioavailability, poor selectivity and high toxicity [19,30,31]. Representative process of gene therapy can be observed in Figure 2.4.

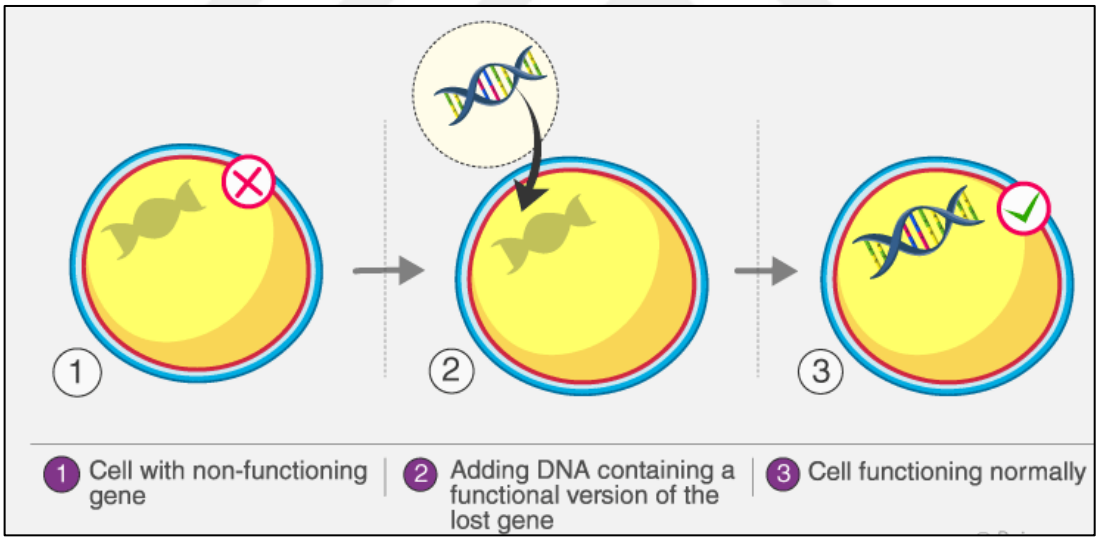

Figure 2.4. Representative process of gene therapy [31]

Currently, there are several strategies that are applied for gene therapy. Induction of apoptosis is the most common technique used in that is applied either by executioner of apoptosis or introducing genes encoding an inducer (32). It has been found that using TNF-related apoptosis inducing ligand (TRAIL) destroy a wide variety of tumor cells and eliminates any harmful effect on normal cells [33]. Melanoma associated gene-7 (mda-7) is an another example of an apoptosis induces, which selectively provokes apoptosis in

different types of cancer via minimal toxic effects on healthy tissues [34]. In addition, at DNA level, the biological function of oncogenes is suppressed and modulated, which can further be used to treat cancer. For instance, a transcription factor MYC, which aims to regulate different cellular processes, can be deregulated in a wide range of human cancers [35]. Another effective approach in gene therapy is the conversion of prodrugs into active compounds in order to exert in-situ cytotoxic effects by presenting genes which encode the converting enzyme which is well demonstrated on a pre-clinical level [36].

Although significant achievements have been made in gene therapy, there are still challanges to overcome such as the selection of most favourable delivery system to target cancer cells, or provide the suitable conditions for optimal expression levels. In addition, gene therapy also exhibits few downsides associated with genome integration, limited effectiveess in some patient subgroups, and also high chances of being neutralised by the immune system [37]. Limited specificity for targeting tumor cells is a common and critical problem associated with those relatively new strategies.

2.1.3.3. Nanotechnology-Based Therapeutics

Although extensive innovations have been made in cancer treatment, some limitations faced as a consequence of cancer treatment approaches, such as cosmetic damage, systemic toxicity, and immunosuppression are still regarded as challanging. These limitations are caused from the lack of selectivity of the therapeutic agent, indiscriminate distribution of drugs and multidrug resistance [38]. In order to alleviate these problems, studies have been focused on drug targeting and delivery of the therapeutics to the cancer region. It is practical to develop drug delivery systems by which cytotoxic agents can be targeted specifically to cancer cells more efficiently. However, the pharmacokinetic profile of conventional chemotherapeutic agents are not sufficient, and those administered also possess serious side effects [39]. Furthermore, the concentration of drug reaches to the tumor site is limited, therefore developing a drug delivery system which delivers the cytotoxic agents directly to tumors site without harming surrounding healthy cells is crucial. The emergence of targeted cancer therapies has become the driving force for developing nanomedicine technologies, where the therapeutic agents can be encapsulated in nano-materials and delivered selectively through the tumor site either

by active or passive targeting mechanisms. Nanotechnology based drug delivery systems provide a convanient way to deliver small molecules in a localized or targeted manner.

Nowadays modern technologies provide opportunities to produce biocompatible nanoparticles with various types of particle size, shape and morphology having unique chemical and physical properties. Nanoparticles have been attracted considerable interest over the last decade for dealing with the restrictions in conventional cancer therapies as they offer excelent benefits for drug delivery approaches. Nanoparticles can also be modified with a variety of materials including polymers, inorganic materials, lipids and also biological materials. Therapeutic agents can be encapsulated within the surrounding matrix or conjugated through functional modifications onto the surface of nanoparticles, where the drug stability, solubility and targeting efficacy can be improved (Figure 2.5). The high surface-to-volume ratio and their allowance for surface modification make nanoparticles to have relatively higher intracellular uptake and to be regarded as more effective drug delivery carriers as compared to microparticles [40,41]. Nano-carriers can maximize drug concentration and its accumulation on tumor tissue while minimizing non-specific uptake thus defends healthy cells from the toxicity effect of drugs. Moreover, enhanced permeability and retention of nanoparticle-based drug delivery system enable to cross through biological barriers by which the circulation time can be prolonged [42].

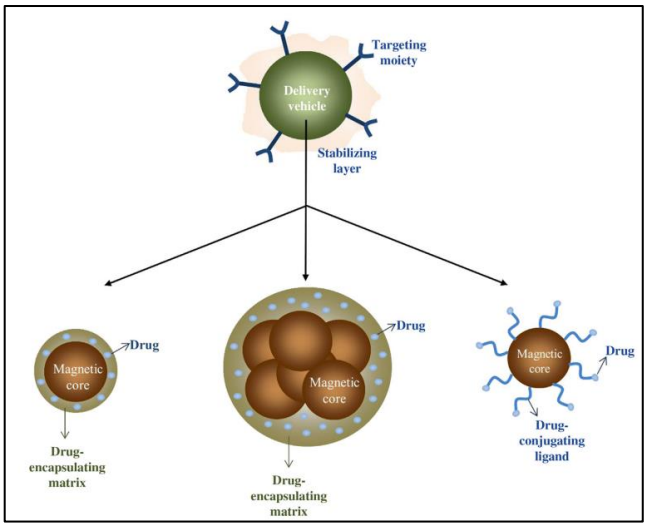

Figure 2.5. Schematics of magnetic nanoparticle based drug delivery systems [3]

The efficiency of nanoparticle-drug delivery system is significantly influenced by the shape, size, and surface characteristics of nanoparticles used in the treatment. For instance, it is well-known that relatively small particles can be easily filtered by kidneys, thus making the usage of nanoparticles ineffective for targeting cancer tissues. On the other hand, it is challenging to deliver larger particles through small capillaries. Moreover, it should be noted that, the bioavailability and half-life of drugs can be adjusted via modifying the surface characteristics of nanoparticles [43]. Thus, factors affecting the efficiency of cancer treatment need to be optimized in order to develop better and efficient targeted nanoparticle-drug system.

Drug delivery systems may also be designed by regarding the properties of tumor ecosystem such that the targeted nanoparticles can be adjusted as either pH-sensitive carriers or temperature-sensitive. The temperature sensitive system carry and release drugs by tracking the change in temperature locally in the tumor site, while the pH sensitive system responds to a specific pH range at the tumor region and delivers the cargo [38].

For effective cancer therapy, drug concentration is preferably to be maximized in the tumor tissue and nano-drug delivery system should be selective to the target cells, while normal cells are protected from cytotoxicity. Drug targeting within the tumor site via nano-carrier can be carried out by passive or active targeting. Indeed, nanoparticles take advantage of the pathophysiological characteristics of the tumor environment and penetrate into the tumor by leaky vasculature and poor lymphatic drainage as a consqeuence of EPR effects [39,40,43–45]s, which is the driving force of passive targeting. Meanwhile, a barrier of endothelial cells is possessed by normal cells in order to obstruct nanoparticle extravasation. Even so, there are some restriction associated with passive targeting considering non-uniform nature of tumor vessels, non-specific drug distribution, and the lack of EPR effect in particular types of tumors [46]. Although the accumulation of the drug can be accomplieshed by the EPR effect, it is not guaranteed to deliver drug within the tumor cells uniformly due to the cellular internalization depending on membrane-specific processes. Thus, significant effort is underway for designing nanodelivery systems which maximize the drug accumulation at tumor site. In contrast, active targeting is based on directing the nanocarriers to the cancer cell by using specific

ligands having affinity solely on the overexpressed receptors of the tumor cells [3]. Active targeting specifically guides the carriers to the tumor site via direct interactions between receptors and ligands. In addition, the surface of nanoparticles can be functionalized with ligands, which are selected for distinguish cancer cells from the healthy cells by recognizing the molecules presenting at surface of cancer cells [13]. The interaction between the receptors on the surface of tumor and ligands on nanoparticles induces receptor endocytosis, that offers nanocarriers to release therapeutic drugs, succesfully [14]. Using this strategy, nanoparticle carrying the drug is delivered to unique and selective subcellular regions with enhanced drug penetration and uptake while preventing the systemic drug exposure for healthy cells. Figure 2.6. shows the fundementals of passive and active targeting of nanopartiles.

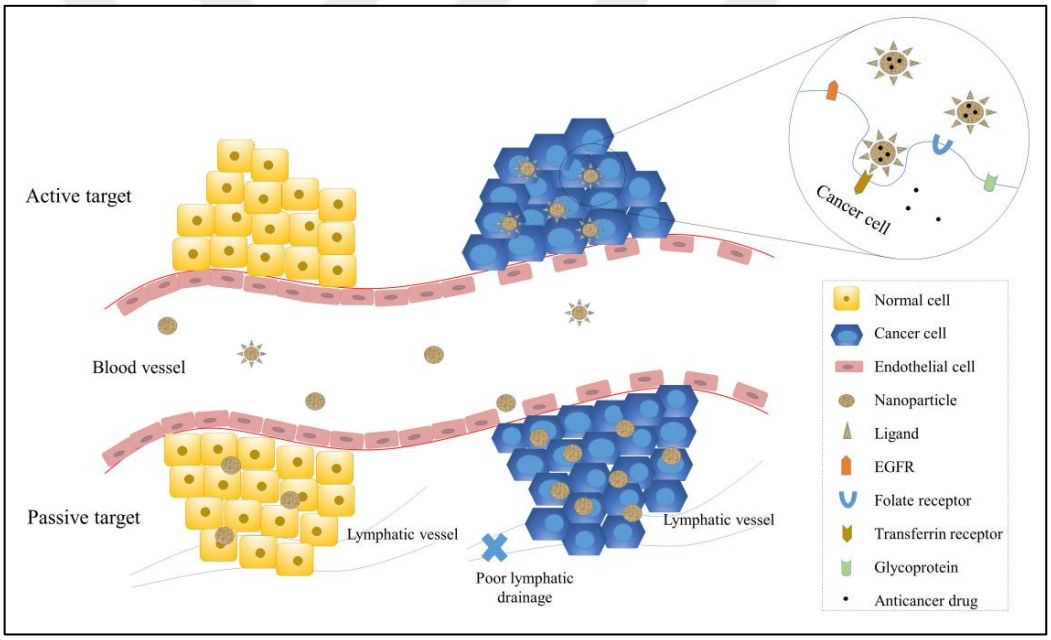

Figure 2.6. Passive and active targeting of nanoparticles [43]

It is possible to transform conventional drug delivery systems into active targeting agents with surface modifications by using ligands, that can be specifically recognized by the surface receptors of cancer cells. Recently, aptamers having high-specificity and affinity are being used as DNA affinity reagents, which are mainly <100-bp nucleic acids, RNA or DNA that can attach to the target such as proteins, drugs, small molecules and cancer cells, through unique 3D strutures as a consequence of their primary sequence [47].

Aptamers exhibit important advantages in terms of reproducible synthesis, small molecular size, low immunity and ability to be easily modified by chemical reactions, which makes them more adaptable and serve as drug carriers [48]. However, aptamers are not ideal for in-vivo applications due to their poor serum stability and small size (25-30kDa) which results in rapid renal clearance from circulation, unless they are connected to a protein or scaffold. After all, adverse effect in binding affinity or specificity can also be arised in the case of attaching them to proteins, or scaffolding by interacting with nanoparticles [17]. In contrast to aptamers, DNA nanoparticulates, which are composed of concatemeric repeats of a sequence, propose a local multivalent platform in a single particle such that performing a wide variety of selection is possible.

2.1.3.4. Hyperthermia

Hyperthermia is a term refers to a therapeutic method for cancer treatment using thermal energy focused on cancer cells with minor effect to surroundings healthy tissues. In hyperthermia treatment, tumor cells are destroyed by increasing the temperature of a region locally to 40-45 ^{o}C causing in the complete or partial destruction by metabolic events including premature (necrosis) or programmable (apoptosis) deaths of malignant cells [3,49]. Hyperthermia is categorized into three submethods: (a) local heating (heat treatment to a small region like a tumor) (b) regional hyperthermia (treating a setion of body such as tissue or organ), (c) whole body hyperthermia (involves heat treatment of cancer cells that are spread to whole body) [50].

Magnetic hyperthermia is a branch of hyperthermia which is applied via biocompatible magnetic nanoparticles (MNPs) as heating sources. When an alternating magnetic field (AMF) is applied to magnetic nanoparticles, heat is released due to hysteresis loss, Brownian relaxation, and Nèel relaxation mechanisms. Brownian relaxation occurs due to the friction arising from the rotation of particles within the carrier liquid whereas Nèel relaxation is resulted from the reorientation of the magnetic moment parallel to the applied alternating magnetic field. Another heating process is the hysteresis loss that takes place as a consequence of magnetic domain wall displacements [49].

The determination of the magnetic nanoparticle’s heating efficiency under alternating magnetic field can be evaluated by specific absorption rate (SAR) which is described as

the rate of heat generation per unit mass of the corresponding magnetic particles, which can be calculated as;

$$SAR\ (\frac{W}{g}) = \frac{C.\rho}{\varphi}.\frac{\Delta T}{\Delta t} \tag{2.1}$$

where, C and ρ is the specific heat capacity and density of water, respectively, φ is the concentration of magnetic nanofluids in mg/mL, and $\Delta T/\Delta t$ represents the maximum heating rate, which can be calculated by conducting a linear fit of time-dependent temperature change data.

Although the usage of SAR parameter has become prevalent with the aim of measuring heating abilities of magnetic nanoparticles in hyperthermia applications, it is quite challenging to compare outcomes from different studies conducted as a consequence of wide variety of experimental conditions and nanoparticle-surface modifier systems. Additionally, most measurements in the literature are carried out under non-adiabatic experimental conditions [5–11,51,52]. Figure 2.7 compares the time-dependent temperature data obtained in the conditions of both adiabatic and non-adiabatic measurements. Since adiabatic measurement systems are challenging to implement and time-consuming, almost all published studies on hyperthermia is conducted under non-adiabatic conditions, either by using homemade systems, or by using commercial devices (i.e. magnetherm by nanoTherics) that offer a wide range of magnetic field amplitudes and frequencies [53].

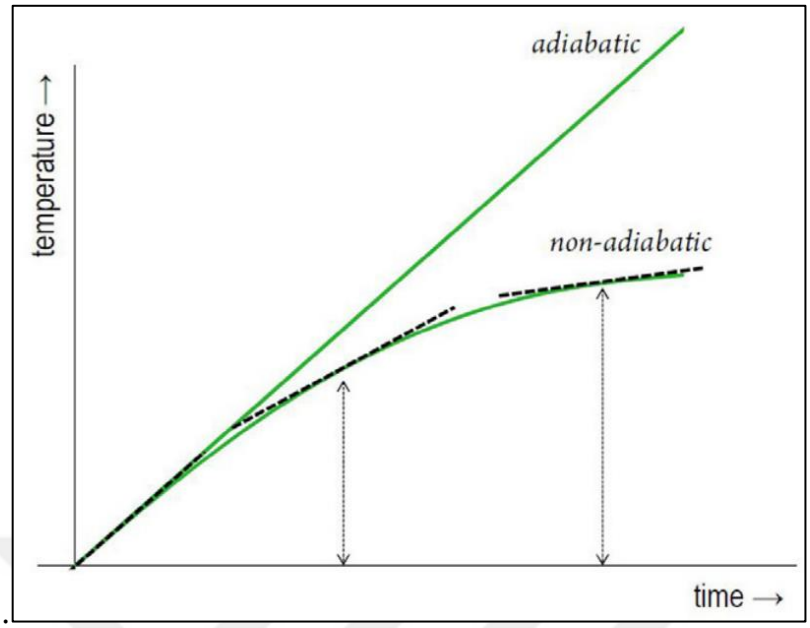

Figure 2.7. Comparison between adiabatic and non-adiabatic conditions of time-dependent temperature change measurements [53]

There are several key factors that influence the heating performance of magnetic nanoparticles and it is essential to investigate those parameters in order to implement these nanoparticles effectively for hyperthermia applications. In general, the significant role of AC magnetic field intensity and frequency over the heat generation of magnetic nanoparticles, has been studied many times. Numerous studies have aggreed that the heating rates and SAR values of magnetic nanoparticles enhance with an increase in both magnetic field amplitude and frequency, as seen in Figure 2.8 [5,11]. However, it must be recognized that, the clinical application of magnetic hyperthermia is restricted by physiological considerations as high magnetic field strength can adversely affect tissues as a result of induced eddy currents. Consequently, Brezovich et al. proposed the physiological limitation of magnetic hyperthermia as a product of magnetic field amplitude (H) and frequency (f) for secure implementation ($Hf < 5\times10^{9}$ $A.m^{-1}s^{-1}$) [54].

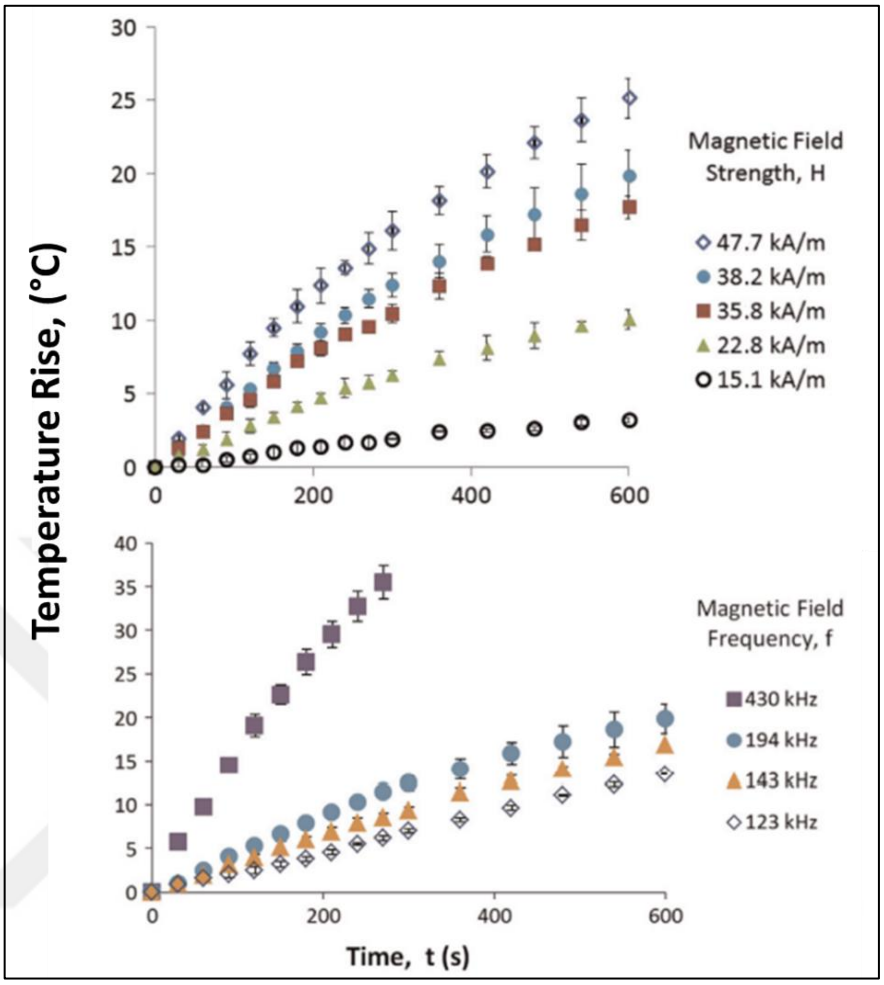

Figure 2.8. Impact of magnetic field amplitude and frequency on local temperature change [5]

Another significant factor that influences the heating generation of magnetite nanoparticles under external magnetic field is nanoparticle size, which affects the relaxation mechanisms. Although there is yet to be a consensus on particle size optimization, it is commonly reported that for relatively larger nanoparticles, hysteresis losses contributes to the heat generation which is amplified by an increase in the ferromagnetic nature [5,6,8]. There is an ongoing discussion in the literature about the effet of concentration on the hyperthermia performance of magnetic nanopaticles. Several studies experimentally investigated the effect of concentration over SAR of magnetic nanoparticles and reported a remarkable decrease in SAR with increasing particle concentration (Figure 2.9) [6–10,51]. It should also be noted that, contradictory studies are present in the literature which state that the SAR is independent of nanoparticle

concentration [5]. In order to improve the hyperthermia performance of magnetic nanoparticles, optimization of the surface coating is another useful approach. Surface coatings not only play an important role in colloidal stability and biocompatibility, but also affect the heating ability of magnetic nanoparticles by changing the viscosity of nanofluids and altering the hydrodynamic size which consequently decrease the effective magnetic properties [52].

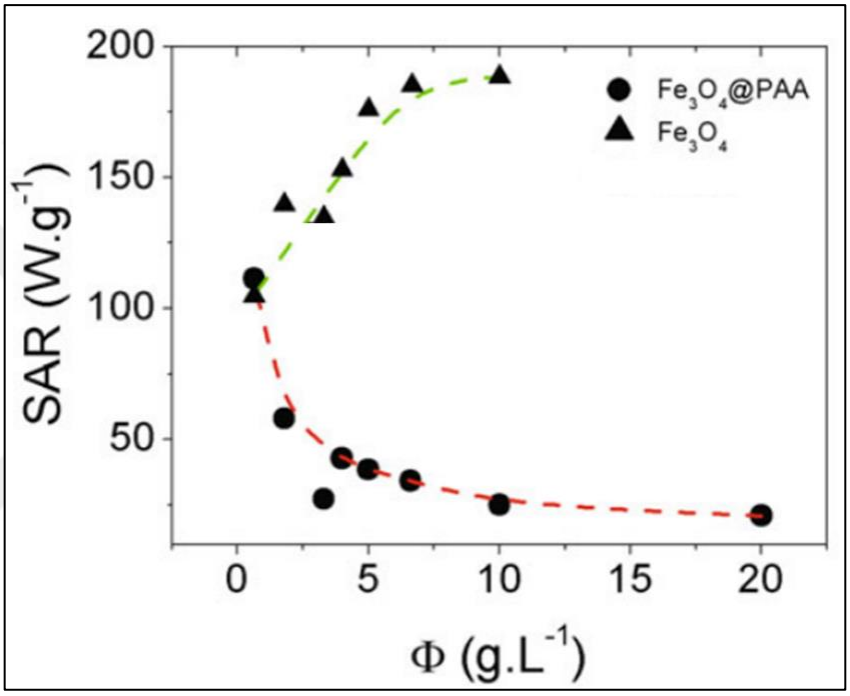

Figure 2.9. Effect of magnetic nanoparticle concentration to specific absorption rate (SAR) of magnetic nanoparticles [7]

Consequently, it is aimed to obtain an effective local temperature increase as well as sufficiently high values of SAR, by using adequate amount of MNP for the optimum application of magnetic hyperthermia. It should also be noted that the hyperthermia efficiency of superparamagnetic nanoparticles has been extensively investigated in the literature, yet, studies on hyperthermia related performance of ferrimagnetic nanoparticles are very few due to complicated colloidal stabilization.

Although maximum amount of SAR is desirable, one of the most challenging problem of magnetic hyperthermia for in vitro and clinical applications is the homogeneous

distribution or selective targeting of nanoparticles at the tumor site. The essential importance of using magnetic nanoparticles in hyperthermia treatment is the ability of manipulating particles via external magnetic field, as seen in Figure 2.10, which can lead to the accumulation and targeting to a specific location within the body thus increase the concentration [55]. Moreover, chemotherapeutic drugs can also be encapsulated on magnetic carriers in order to facilitate effective drug delivery system while preserving the surrounding healthy tissue, as well as boosting the effectiveness of hyperthermia treatment [56,57].

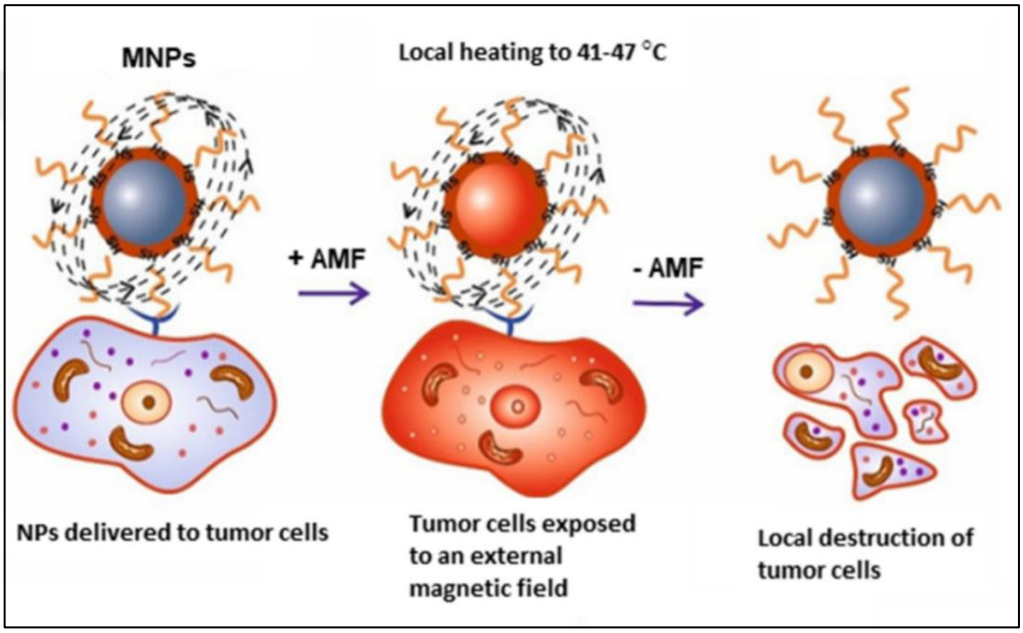

Figure 2.10. Schematic representation of magnetic hyperthermia [50]

MNPs can be delivered specifically to the tumor site for effective hyperthermia therapy in three main approaches: direct injection, passive and active targeting. One of the most simple way to administer the MNPs is the direct injection, where magnetic nanofluids are directly injected into the tumor site [49]. By using intratumoural injection, MNPs can be delivered in the tumour with high and localised concentrations. Nevertheless, high chances of non-homogeneous MNPs distribution at the tumour site as a result of direct injection is a drawback [12] as heterogeneous distribution of magnetic nanoparticles within the tumor reduce the therapeutic efficiency. On the other hand, passive targeting is based on injecting MNPs intravenously that will accumulate in tumor tissue,

preferentially, as a result of EPR effect. The systematic delivery of nanoparticles with passive targeting results in more global distribution of MNPs at the tumor tissue, as compared to direct injection. However, the major disadvantage of passive targeting is the challenge of achieving a sufficient MNP concentration for efficient treatment, while the amount of injected nanoparticles must be kept at optimum in order to avoid non-negligible MNP toxicity. Therefore, lack of desired nanoparticle concentration leading to inadequate heating in local region makes the magnetic hyperthermia treatment ineffective. In contrast, active targeting is the modification of nanoparticle surface with targeting ligands that have the ability to recognise and attach to cell receptors, which results in enhanced accumulation in the targeted site leading to higher particle uptake while deteriorating the side effects to healthy cells [49]. Although, the superiority of targeted MNPs in magnetic hyperthermia has already been proposed many times, there are some studies both in-vitro and in-vivo [58,59], suggesting poor heating performance of MNPs as a consequence of insufficient amount of particles that are delivered to tumor site by active targeting [60,61].

2.2. MAGNETITE

Magnetite is a type of iron oxides and the most naturally occuring magnetic mineral with the chemical formula Fe_3O_4 which contains both Fe^{3+} and Fe^{2+} ions in a 2:1 stoichiometric ratio (Figure 2.11) [62].

Figure 2.11. Magnetite (Fe3O4) Minerals [63]

Magnetite has an inverse spinel crystal structure, which consist of iron ions occupying 16 octahedral and 8 tetrahedral positions in a face centered cubic (FCC) close-packing of oxide (O_2) ions. The Fe^{2+} ions favourably occupy octahedral sites as a result of their unique crystal field stabilization energy, whereas the Fe^{3+} are equally distributed between octahedral and tetrahedral sites. In the ground state, Fe^{2+} ions have two paired and four unpaired 3d electrons, while Fe^{3+} ions contain five unpaired electrons in their d orbitals. Consequently, the electron spins do not cancel-out each other leading to a lattice with a net magnetic moment [62]. The magnetic properties such as the type and saturation magnetization of magnetite nanoparticles are highly affected by the average size of particles. When the average size of particles are less than 20 nm, the particles have superparamagnetic behavior where particles align themselves according to the applied magnetic field direction but in the absence they do not have any remaining magnetization. However, for larger particles ferrimagnetic properties are governing in which the particles tend to attain remaining magnetization even in the absence of an externally applied magnetic field. It should also be noted that these particles have relatively larger saturation magnetization as compared to superparamagnetic counterparts.

2.2.1. Synthesis Methods of Magnetite Nanoparticles

There are numerous chemical synthesis pathways for the production of magnetite nanoparticles affecting versatile properties of average particle size, morpholgy, crystallinity and also colloidal stability. Briefly, co-precipitation, partial oxidation and thermal decomposition are the most preferred methods for preparing magnetite nanoparticles.

2.2.1.1. Coprecipitation Method

Probably, the co-precipitation method is the simplest and most common aqueous chemical pathway to obtain magnetite nanoparticles. It is based on the stoichiometric mixing of ferric and ferrous ions (2:1) in an inert atmosphere followed by the addition of base for regulating the pH and precipitating the particles. The typical reaction mechanism of magnetite formation (Fe_3O_4) via co-precipitation is as follows.

$$Fe^{+2} + 2Fe^{+3} + 8OH^{-} \rightarrow Fe_3O_4 \quad (2.1)$$

The essential advantages of this method are the possibility to synthesize magnetite nanoparticles in a relatively faster manner and without using complex reaction mechanisms, which yields nanoparticles with relatively smaller average sizes (8-10 nm) and exhibit superparamagnetic properties which show no net magnetization in the absence of an external magnetic field. In addition, surfactants and polymers can easily be incorporated into the reaction pathway to prevent aggregation of nanoparticles and achieve colloidal stabilization. On the other hand, it is challenging to control the morphology and size distribution of particles due to fast reaction kinetics [64].

2.2.1.2. Partial Oxidation Method

Magnetite can also be obtained via the gradual oxidation of Fe^{2+} ions in the presence of an oxidant at higher pH. Magnetite nanoparticles prepared by this technique have a mean particle size between 40 and 50 nm, and exhibit ferrimagnetic properties at room temperature. As a consequence of strong magnetic interactions, achieving the colloidal stability of those nanoparticles in aqueous medium is challenging which is a necessity for biomedical applications [64,65].

In partial oxidation, ferrous hydroxide is partially oxidized to the intermediate product called green rust, which is further oxidized to form magnetite nanoparticles. The reaction is conducted in an inert atmosphere in order to inhibit further oxidation of magnetite to other iron oxides such as maghemite or goethite [65]. The larger particles obtained via partial oxidation is a result of relatively slower reaction kinetics as compared to co-precipitation method. Differences in the morphology of magnetite nanoparticles according to their synthesis route can be observed in Figure 2.12.

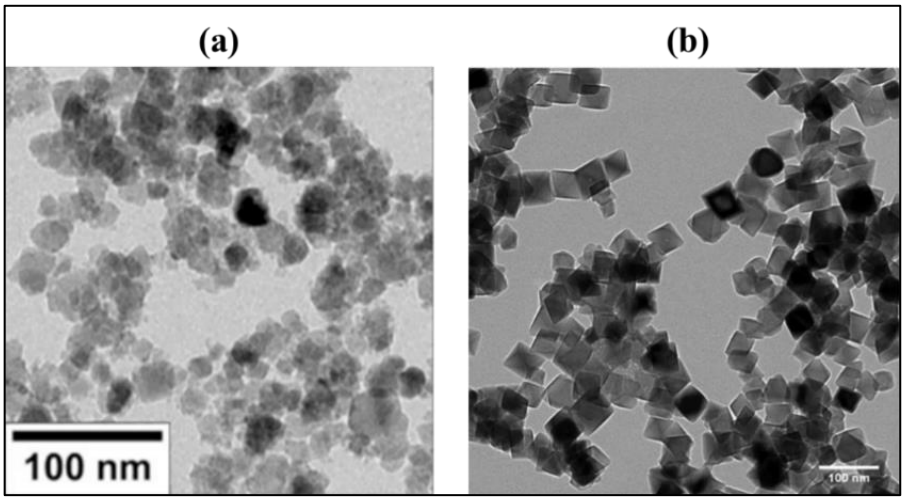

Figure 2.12. Transmission Electron Microscopy (TEM) image of Fe3O4 nanoparticles synthesized by (a) co-precipitation (b) partial oxidation method [64,65]

2.2.1.3. Thermal Decomposition Method

In this method, iron precursors are decomposed at elevated temperatures in organic solvents in the presence of stabilizing and reducing agents such as oleylamine and oleic acid. High quality magnetite nanoparticles with sizes ranging from 3 to 20 nm can be obtained using thermal decomposition method [64].

2.2.2. Characterization of Magnetite Nanoparticles

It is essential to characterize synthesized nanoparticles to quantify and specify their structure, composition, average size, morphology as well as magnetic properties for their implementation in various applications as these properties may vary depending on the synthesis route and parameters affecting the corresponding mechanism [66]. The phase identification of magnetite nanoparticles is generally accomplished via X-ray diffraction (XRD) or selected area electron diffraction (ED) by matching the diffraction angles or d-spacing values with databases given in the literature. Raman or Mössbauer spectroscopy can also be used as complementary methods, since the crystal structures of some iron oxides such as magnetite and maghemite are similar and challenging to distinguish via XRD. Transmission electron microscopy (TEM) is used to demonstrate particle size, morphology and size distribution of magnetite nanoparticles while vibrating-sample

magnetometer (VSM) is used to measure the saturation magnetization, coercivity and remanance of particles for revealing the magnetic properties of nanoparticles. Finally, the thermal stability of nanoparticles can be evaluated via thermogravimetric analysis (TGA) which also yields information about the presence of surface active agents and/or polymers that are used for achieving colloidal stability in aqueous medium or further functionalization by comparing the corresponding decomposition temperature of these organic molecules.

2.2.3. Biomedical Applications of Magnetite Nanoparticles

Magnetite nanoparticles are highly utilised in biomedical applications thanks to their excellent magnetic properties, biodegradability and biocompatibility. They can be applied in MRI for visualization, plus their ability to be targeted to a specific region via an external magnetic field enables magnetite particles to play an major role in delivery systems. Also, magnetite can be implemented in hyperthermia applications as heating sources which can emerge under an externally applied alternating magnetic field.

Indeed, there are several parameters that affect the toxicity of nanoparticles such as physical and chemical properties, the biological behavior and administration protocol including the dose. Consequently, the toxicity and biocompatibility of magnetite nanoparticles should be carefully examined in-vitro and in-vivo for expressing the safe application of these nanoparticles in biomedical applications. Several applications that are used magnetic nanoparticles are presented in Figure 2.13.

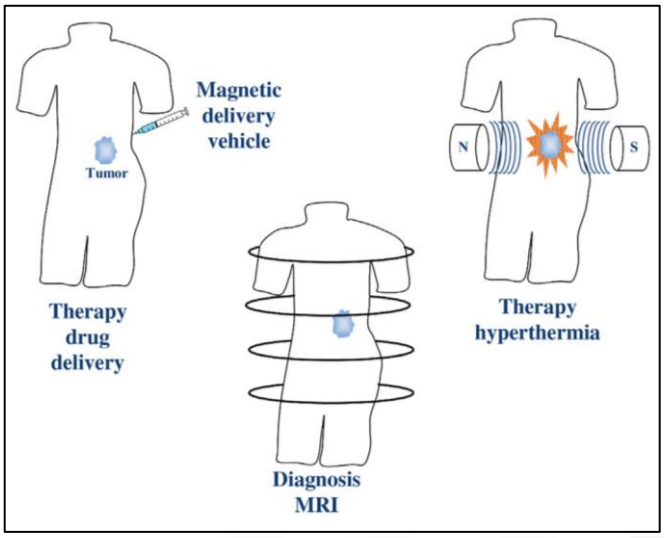

Figure 2.13. Different implementations of magnetic nanoparticles in biomedical applications [3]

One of the most well-known visual diagnostic tool is magnetic resonance imaging (MRI, which can be applied primarily to create high-resolution images of tissues in 2D and 3D. The principle of MRI relies on magnetic resonance, where constrast agents are required to enhance its sensitivity and sharpness for detecting various pathological processes. As mentioned before, magnetite nanoparticles exhibit strong magnetism and this behavior make them efficient candidates as reliable contrast agents. At a tissue of interest, the transverse relaxation time is shortened as a result of higher magnetic susceptibility of magnetic cores. Thus, darker MR image can be obtained as a consequence of magnetite nanoparticles localization at the targeted site [3,67,68].

The application of Fe_3O_4 nanoparticles for delivery purposes has gained attention over the years. A distinctive advantage of magnetite nanoparticles is their capability to be guided/targeted to the cancer cell by using an externally applied magnetic field which cause to concentrate additionally the attached chemo drug. While magnetic particles are preferred due to unique magnetic properties for suitable manipulation in the presence of an magnetic field, it is essential to functionalize the magnetite nanoparticles with a proper coating or a matrix in order to inhibit clogging of small capillaries or blood channels (Figure 2.14). The outer shell, or matrix, not only improves the functionality of magnetite nanoparticles through encapsulation of drug and binding molecules, but also delays

uptake by the mononuclear phagocyte system [69]. Up to date, several stimuli-sensitive and selective magnetite based nanocarriers for drug delivery have been conjgated with different chemotherapeutic agents, including cisplatin [69], doxorubicin [70], paclitaxel [71], gemcitabine[72], idarubicin[73], etc.

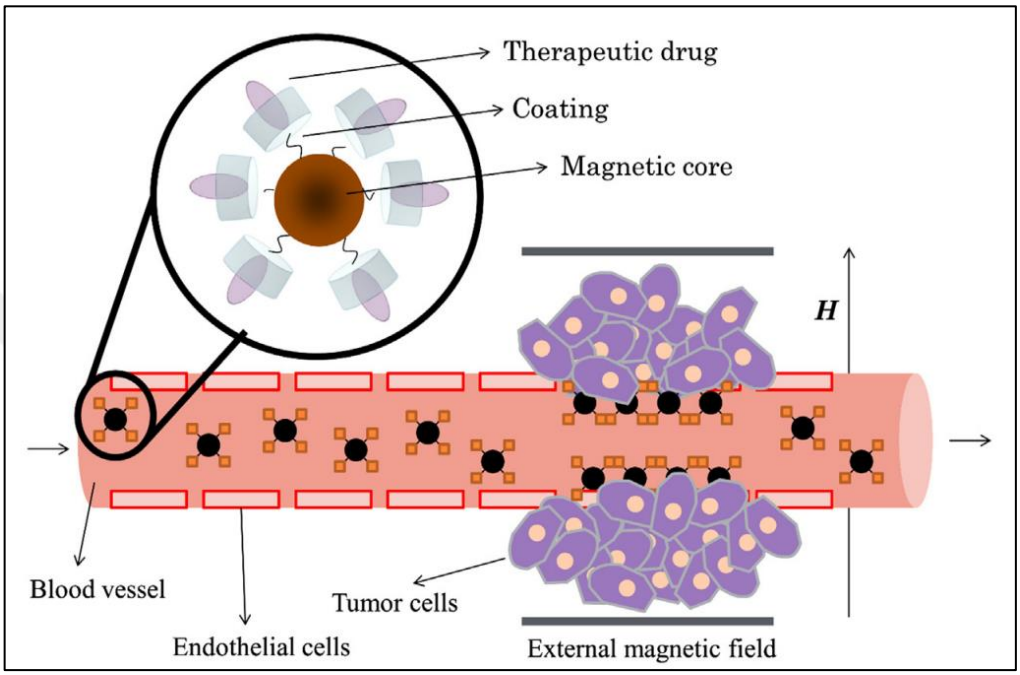

Figure 2.14. Magnetic nanoparticles as a drug-delivery agents under an external magnetic field [3]

Over the last decades, magnetic hyperthermia has been numerously studied both in-vivo and in-vitro applications by using magnetite nanoparticles as heating sources. Asin et al [74] investigated the hyperthermia performance of superparamagnetic magnetite nanoparticles functionalized with dextran by considering the death rate of dendritic cells as a function of particle concentration and exposure time. Their report indicates the necessity for the optimum conditions of magnetic field properties for effective magnetic hyperthermia applications. Ghosh et al [4] reported 65 percent reduction in breast cancer cells (MCF-7) that can be achieved by using oleic acid & PEG functionalized magnetite nanoparticles. Also, Guardia et al [75] presented the heating performance of PEG-coated MNPs having various particle sizes, as a function of alternating magnetic field amplitude and frequency. The highest values of SAR (2452 W/g) was recorded at a condition of 29kA/m and 520 kHz and almost 50 percent mortality of KB cancer cells was observed.

Furthermore, magnetic hyperthermia has been combined with conventional treatments such as chemotherapy for enhancing the efficiency. For instance, magnetite nanoparticle polymeric micelles prepared by the conjugation of poly(ethylene glycol)-poly(lactide) were examined as nanocarriers of doxorubicin (DOX) by Kim et al. [76]. They reported that 78 percent of the A549 cancer cells were destroyed by both the consequence of heating and toxicity effect of drug.

2.3. DNA (DeNAno) NANOPARTICLES

2.3.1. Introduction to DeNAno

Compared to conventional biopolymers, DNA has an exclusive overlapping functional and structural activities. DNA motifs can behave either as a ligand to specific biomolecules, or as a scaffold for oligonucleotide conjugation to hybridize oligonucleotide conjugates [17]. DNA can be chemically modified to allow metal ion binding, or to carry DNA binding drugs [77]. Favorable toxicity, biodegradability profile and specificity of DNA make it as a potential affinity reagent for delivery system and therapeutic applications.

Rolling Circle Amplification (RCA) is an isothermal, enymatic polymerization process mediated by suitable DNA polymerases that utilizes circular oligonucleotide templates in order to produce long single-stranded DNA (ssDNA) with a repeating sequence units. The RCA-produced long, concatemeric oligonucleotide template is referred as DNA nanoparticles (DeNAno) [16]. Each DNA nanoparticle consist of thousands of copies of template, and libraries contain > 10^{10} unique particles. The resulting DeNaNo particles are concatemers with complementary sequence to the circularized oligonucleotides. Each nanoparticle exhibit specific 2D and 3D structures due to its randomized nucleotide sequence, which allows DeNano libraries are considered as diverse binding agents pools that attach to different complex surfaces. It is possible to conjugate of DeNano nanoparticles with molecular cargo, directly [16,17].

In the selection process, the diverse library of DeNAno is incubated with a target like cells, proteins or small molecules. After discharging unbound particles, DNA

nanoparticles are re-amplified with PCR method by symmetric PCR followed by asymmetric PCR by using 5’ and 3’ primer sites, and new DeNAno particles are generated via ligation/circularization of enriched template strand. The selection process is repeated until high-binding clones dominate the pool [17].

In cancer treatment, a significant challange is the lack of suitable binding reagents that target cancer cells without binding normal, healthy cells. On the other hand, selected DeNAno nanoparticles may bind to an array of cell-surface receptors without a prior knowledge of the target surface molecules. Initial selections with DeNAno were performed with primary human dendritic cells [16]. Moreover, it was reported that DeNAno particles can specificaly bind to pancreatic cancer cell line, Panc-02 [17].

The unique properties of DeNAno libraries propose a novel approach to cell affinity reagents which replaces high affinity binding characteristics to specific targets with a diverse landscape of high-avidity interactions.

2.3.2. Synthesis and Characterization of DeNAno

A two-step protocol was conducted for the production of DeNAno nanoparticles, mainly based on the RCA method. In the first step, the 100 bp long C39 complementary DNA sequence having specific affinity for the Panc02 cell line was circularized with the help of a 40 bp long semi-complementary intermediate sequence. This phase consist of bonding and hybridization processes. In the next step, this circular DNA sequence was utilized as a template and DeNAno nanoparticles were produced by RCA method. The RCA method consists of four different processes as initiation, elongation, chain displacement and DeNAno formation. The production steps of DNA nanoparticles are represented in Figure 2.15 and extensive details of the synthesis and purification steps of DeNAno can be found in previous studies [16,17,78].

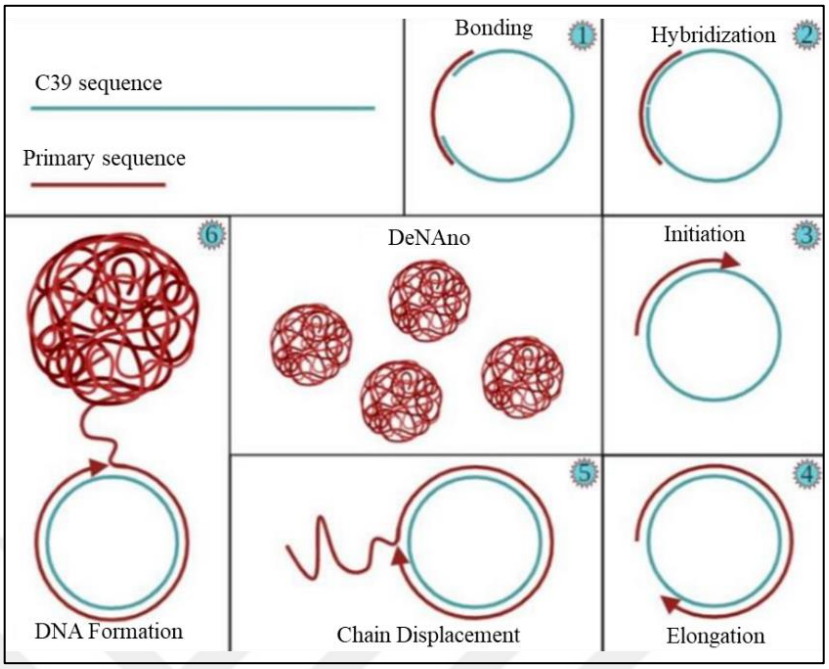

Figure 2.15 Production steps of DeNAno nanoparticles [79]

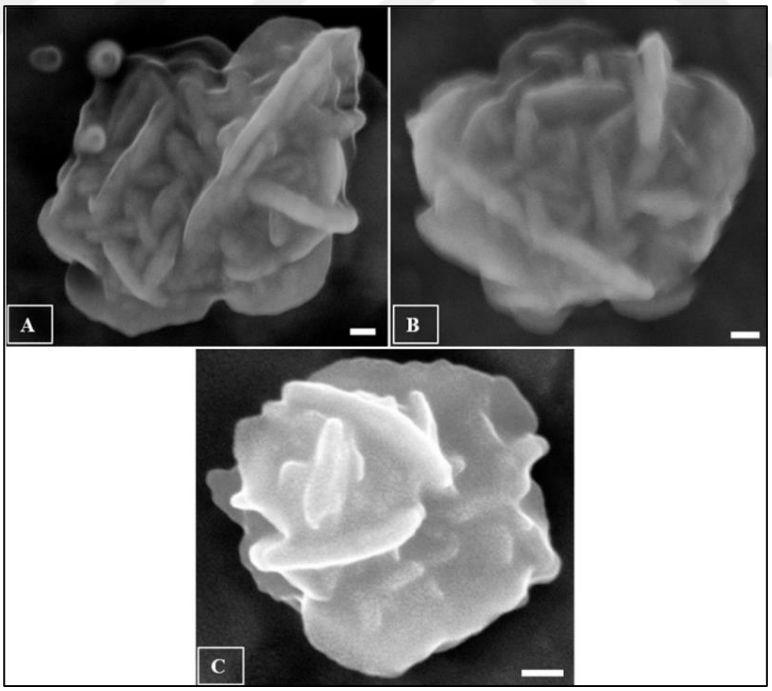

Figure 2.16. DeNAno nanoparticles having different reaction times (A) 15-minutes (B) 30-minutes,(C) 60-minutes [79]

The size and morphology of DeNAno particulates synthesized via RCA method was investigated by using scanning electron microscope (SEM) and the average size of DeNAno was found in between 200 nm – 600 nm (Figure 2.16).

2.3.3. Conjugation of DeNAno and Magnetic Nanoparticles

Conjugation of DeNAno with magnetic nanoparticles was carried out in two steps. In the first step, a binder sequence that is fluorescently labeled binder sequence (FAM) complementary to DeNAno was conjugated with MNPs. In the following step, by using this intermediate sequence, MNP was binded to DeNAno particulates.

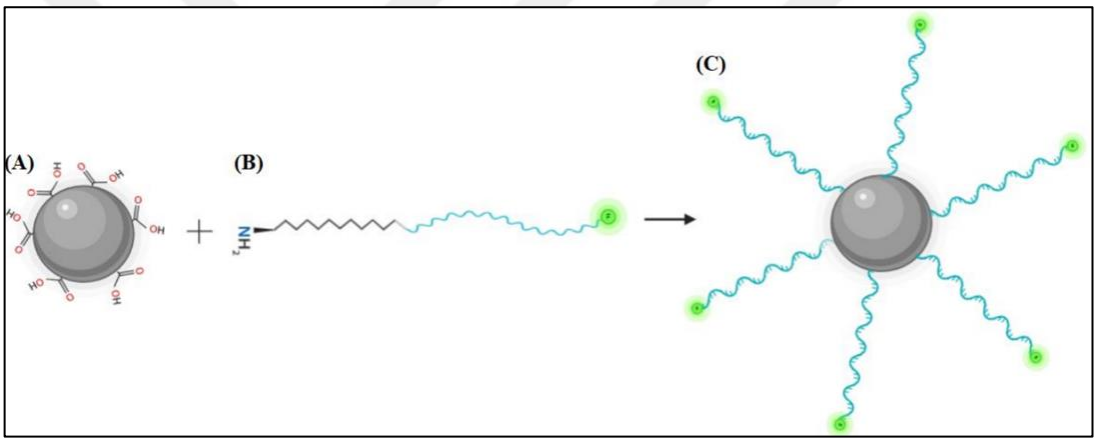

Figure 2.17. Schematic illustration of the conjugation of MNP with the fluorescent labeled binder sequence using the EDC/NHS method (A) MagNP nanoparticles having -COOH groups on the surface (B) Complementary binder with fluorescent property (FAM) (C) MNP/FAM with many complementary binding sequences attached to its surface [79]

Integration of the DeNAno-complementary binderintermediate sequence (FAM) into magnetite nanoparticles is based on EDC/NHS chemistry. This chemical method involves the bonding of the NH_2 group at the end of the complementary intermediate sequence with the carboxyl group (-COOH) onto the surface of MNPs coated with the polyacrylic acid (PAA), leading to the elimination of a water molecule (H_2O) and formation of an amide bond between these two functional groups (Figure 2.17).

Conjugation of DeNAno with magnetite nanoparticle (MNP) was carried out in two steps. In the first step, magnetic nanoparticles were covalently bonded via EDC-NHS chemistry with a binder sequence (FAM) that is known to be complementary to the oligonucleotide sequence of DeNAno while in the second step of process, DeNAno was allowed to conjugate to the complementary intermediate sequence with weak hydrogen bonds. The resulting DeNAno-MNP/FAM conjugation acquired fluorescence characteristic due to FAM presenting on the complementary intermediate sequence which are conjugated with MNP (Figure 2.18). The obtained DeNAno-MagNP/FAM conjugate was imaged via confocal microscopy as a consequence of fluorescent properties as shown in Figure 2.19 and the results indicated the successfull attachment of magnetic nanoparticles onto DeNAno particulates.

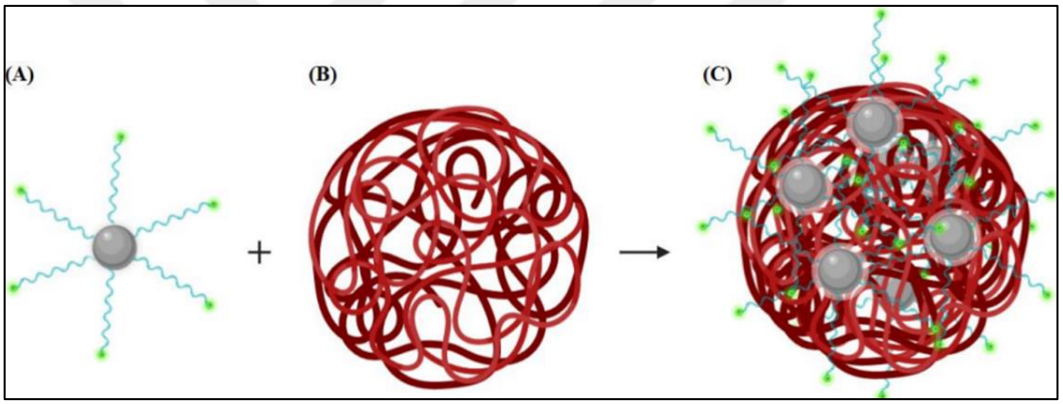

Figure 2.18. Conjugation of DeNAno and MNP with the aid of a complementary binder intermediate sequence (A) MNP/FAM conjugate, (B) DeNAno, (C) DeNAno-MNP/FAM conjugate [79]

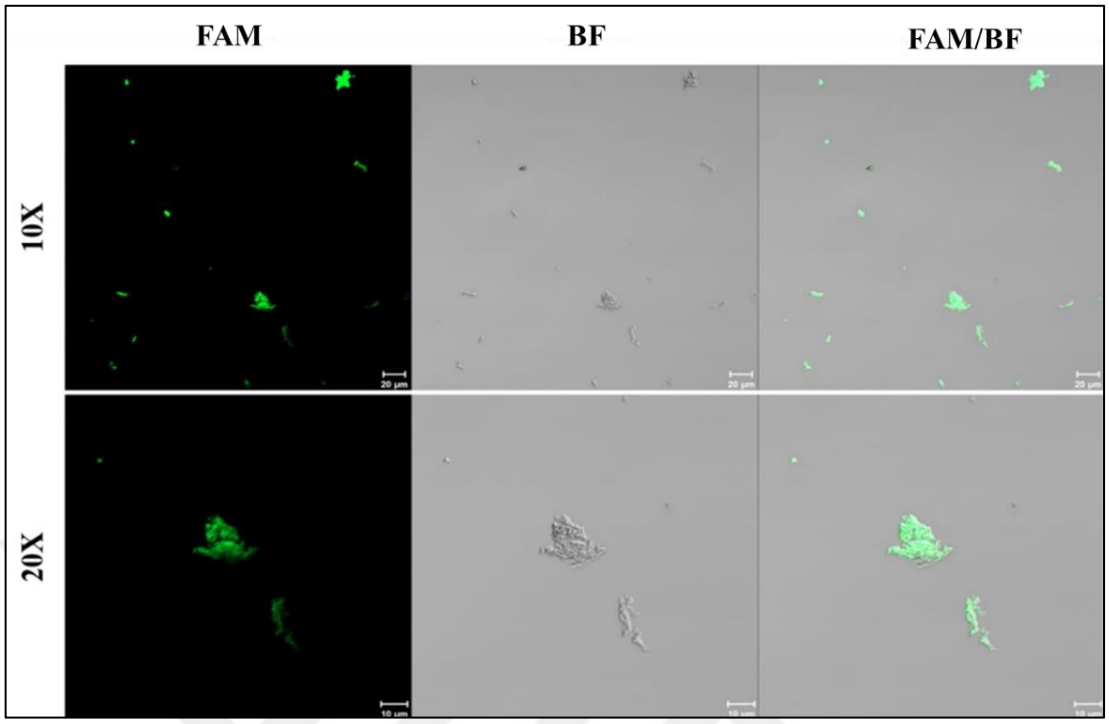

Figure 2.19. Visualization of DeNAno-MNP/FAM conjugate under a confocal microscope, FAM: Fluorescent image, BF: Bright field, FAM/BF: Combination of FAM and BF images, bar length: 5 µm [79]

2.3.4. Cell Selectivity Experiments

Panc02 murine pancreatic cancer (Mus musculus, pancreatic ductal adenocarcinoma, epithelium) and Panc1 human pancreatic cancer (Homo sapiens, pancreatic ductal carcinoma, epithelial) cell lines were used for cell culture experiments. In order to demonstrate the selectivity of DeNAno produced with the C39 sequence to the Panc02 cell line, analyzes were conducted with the Panc02 murine pancreatic cancer cell line and the Panc1 human pancreatic cancer cell line.

The indicated cells were incubated with magnetite-conjugated DeNAno particulates and the conjugates that were not attached onto the cells were washed away from the medium. The remaining conjugates along with cells were finally imaged via confocal microscopy. The results illustrated that DeNAno particulates retain their specific binding affinities to cell lines even after conjugation with magnetite nanoparticles (Figure 2.20). This outcome has presented the possibility of implementation of DeNAno-MNP conjugates in

biomedical applications such as magnetic hyperthermia where specific binding to cancer cell lines is intented.

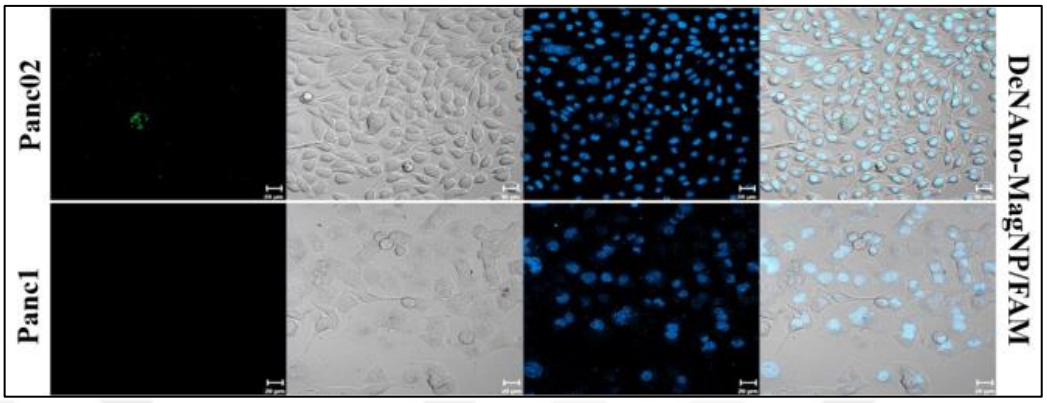

Figure 2.20. Visualization of MNP and MNP/FAM conjugate under a confocal microscope, FAM: Fluorescent image, BF: Bright field, FAM/BF: Combination of FAM and BF images, bar length: 5 μm [79]

All in all, unsatisfactory outcomes in cancer treatment are generally caused from the nonuniform distribution of magnetite nanoparticles within the tumor site and adversely affect to healthy tissues due to unfavorable concentration. Thus, more localized treatment methods are aimed to be developed by considering target specific agents that can diagnose and selectively attach to tumor cells as well as unaffecting the healthy tissues. In this project, DeNAno particulates, that were synthesized via RCA process, can be succesfully conjugated with magnetite nanoparticles which offers an innovative way to deliver magnetic nanoparticles to cancer cells and attain uniform distribution in order to avoid unfavorable concentrations, as well as to enhance the efficiency of hyperthermia treatment.

3. MATERIALS

For the synthesis of magnetite nanoparticles via partial oxidation method, ferrous sulfate heptahydrate ($FeSO_4.7H_2O$) and Polyacrylic acid (Mw: 250kDa & 450kDa) were acquired from Sigma Aldrich. Potassium nitrate (KNO_3) and potassium hydroxide (KOH) were obtained from Isolab and Emsure, respectively. Tiron (98.5 percent) and 38 percent HCl were purchased from Fluka and Sigma Aldrich, respectively, for the determination of iron content of the synthesized magnetic nanofluids.

4. METHODS

4.1. SYNTHESIS OF MAGNETITE NANOPARTİCLES

Magnetite nanoparticles were synthesized via partial oxidation method in which Fe^{2+} ions are gradually oxidized in the presence of an oxidant at high pH. Briefly, 2.525g of KNO_3 and 0.974g of KOH were dissolved in 118.75mL of distilled water and transferred into a round bottom flask. Both reaction mixture and additional 6.25mL of distilled water were de-aerated simultaneously for 60 minutes under inert atmosphere. Following the degassing process, 0.8685g of $FeSO_4.7H_2O$ was dissolved in previously deaerated water (6.25 ml) and directly injected into the reaction mixture containing the base and the oxidant. Then, the overall reaction mixture was bubbled with nitrogen for another minute and the flask was placed on an oil bath which was preheated to 90 ^oC. After 4 hours of mixing, the reaction mixture was cooled down to room temperature and the particles were collected via centrifugation (6000 RPM). The collected particles were washed several times with distilled water and dried in a vacuum oven (60 ^oC) for further characterization. In order to achieve colloidal stability, polyacrylic acid(PAA) with different molecular weights (250kDa & 450kDa) were inroduced into the initial solution where KOH & KNO_3 were present and the amount of polymers were adjusted according to the ratio of the iron ions present to the functional groups of PAA. For the magnetic nanofluids Tiron chelation test [80] was carried out to determine the concentration of magnetite nanoparticles.

4.2. DETERMINING MAGNETITE CONCENTRATION

After the reaction is carried out, Tiron chelation test was conducted for determining the iron concentration of magnetic nanofluid samples with unknown concentrations. Tiron is a chemical compound used for its capability to form strong complexes with titanium and iron. In Tiron test, firstly ferrous and ferric ions are liberated by the addition of concentrated hydrochloric acid solution. The addition of acid also serves for removing the surface coating around the particles. Then, Tiron forms a complex with iron at a ratio

of three Tiron molecules to each iron ion. For samples having a pH greater than 9, complex exposes a strong absorbance at 480 nm. Thus, a sodium hydroxide solution is added in the subsequent step. The instantaneous color change from yellow to red shows the chelation of liberated iron ions with the Tiron molecules [80]. The absorbance of the obtained solution is determined at 480 nm by using spectrophotometer. Finally, using the obtained absorbance value, the unknown concentration of the magnetite sample can be calculated by using equation 5.1 in which DF is the dilution factor.

$$Concentration\ \left(\frac{g}{mL}\right) = \frac{(ABS@480\ nm) \times (DF) \times 231.52 \times 25}{39986 \times 162.15 \times 3 \times 0.1} \quad (4.1)$$

In this test, a small amount of magnetic fluid (0.1 mL) and 0.4 mL of hydrochloric acid (37 percent) was put into a 25 mL volumetric flask and mixedin the purpose of liberating ferrous and ferric ions. Then, by using heat gun, the solution was heated for a few seconds until the yellow color is observed. The mixture was allowed to cool down to room temperature. Then, 0.6 mL of Tiron solution (0.083 g/mL) was added into the mixture in order to form complex structure. Then, the solution color was turned to red by the addition of 3 mL of 4 M sodium hydroxide. The absorbance of this solution was measured using a UV-Vis Spectrophotometer at λ=480 nm.

4.3. CHARACTERIZATION OF MAGNETITE

The morphology and average particle size of nanoparticles were investigated using transmission electron microscopy (TEM) with a 200keV JEOL JEM-ARM200F microscope. Also, average particle size and size distribution were determined by computing the long and short axis sizes for at least 100 individual particles using ImageJ and Gatan Digital Micrograph softwares. The average size of each particle was determined by taking the average of the measured short and long axis dimensions, and then the size distribution was constructed. In addition, high resolution and magnification TEM images were also taken as complementary to the XRD analyzes that will be used to reveal the crystallinity and phase determination of the nanoparticles. The d-spacing values

of individual particles were determined by using Gatan Digital Micrograph. Briefly, a particle with a definite crystal lattice is selected. Afterwards, the FFT (Fast Fourier Transform) algorithm was used to determine the d-spacing values. The distances of the points to the center were determined and the d-spacing values were calculated and compared with the d-spacing values given for magnetite phase in the literature.

The crystal structure of sythesized nanoparticles were specfied by X-ray diffraction (XRD) via Rigaku D-Max 2200 PCI diffractometer with Cu Kα radiation. The X-ray patterns were collected between 10° and 80° at room temperature for dried nanoparticle powders, which were obtained following a lyophilization process. The intensity ratios, d-spacing and 2Θ values corresponding to the peaks of the obtained XRD patterns were compared with the theoretical pattern given for magnetite in the literature.

Electron diffraction pattern of bare nanoparticles synthesized by partial oxidation method was obtained by TEM. This pattern was obtained from a region with a high population of particles, then Digital Micrograph software was used in order to find the center of the diffraction pattern. Then, the diffraction pattern were analyzed with the diffraction tools plugin of the ImageJ software, and the signals were converted to radial distributions. Peaks in the obtained radial distribution were determined separately and compared with the d-spacing values found in different iron oxide species and their corresponding intensities.

Dynamic light scattering (DLS) was performed using a Malvern Zetasizer Nano ZS instrument to obtain the hydrodynamic size distribution and the zeta potential of magnetite nanoparticles for interpreting the colloidal stability.

Thermogravimetric analysis (TGA Perkin Elmer Pyris 1) was performed in an N_2 atmosphere to determine the existence of organic molecules attached on the surface functionalized magnetite nanoparticles synthesized via partial oxidation method. Particles were allowed to heat from room temperature up to 600ºC, at a heating rate of 10ºC /min.

Vibrating sample magnetometer (VSM Quantum Design) were used at room temperature in order to evaluate the magnetic properties and the saturation magnetizaton of both functionalized and bare magnetite nanoparticles and at dried state between -30 and +30 kOe. After the measurements, it was possible to determine whether the synthesized

magnetite nanoparticles exhibit superparamagnetic or ferimagnetic properties, as well as their saturation magnetization. Since magnetite nanoparticles synthesized by the partial oxidation method are expected to exhibit ferimagnetic properties VSM analysis was also expected to reveal the corresponding coercivity and remenance of magnetic nanoparticles.

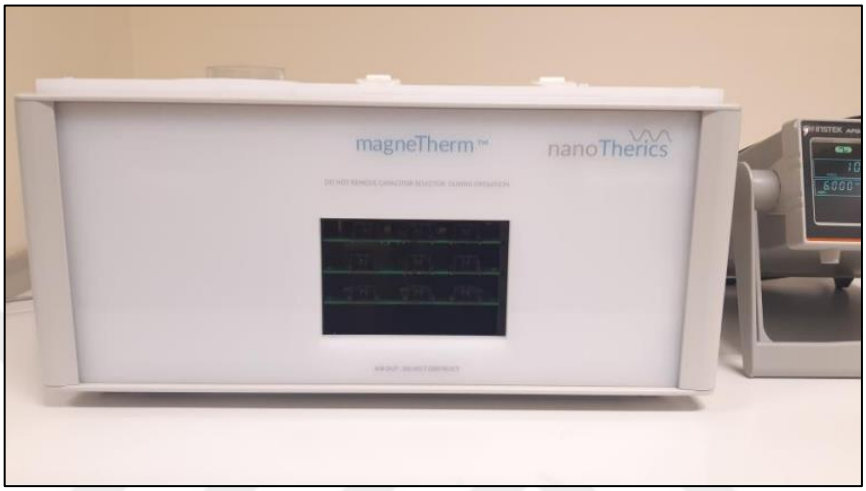

Figure 4.1. magneTherm hyperthermia testing device (nanoTherics)

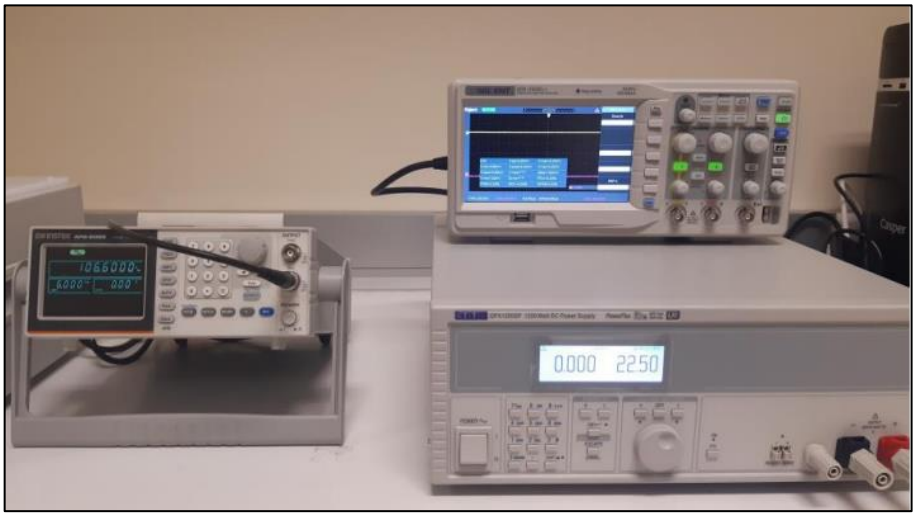

Figure 4.2. Control units that regulate the magnetic field amplitudes and frequencies

The efficiency and performance of ferrimagnetic magnetite nanoparticles in hyperthermia applications were conducted via calorimetric method using the nanoTherics MagneTherm system (Figure 4.1 and Figure 4.2). Fiberoptic temperature sensor was used in order to

efficiently record the change in temperature that is generated by the magnetite nanoparticles under externally applied alternating magnetic field. Two different coil systems (9 and 17) can be used to apply magnetic field frequencies ranging from 100 kHz to 1MHz and various magnetic field amplitude by altering capacitor type. In this way, hyperthermia performance (SAR measurement) of magnetic nanoparticles can be determined within the magnetic field and frequency ranges given in Table 4.1.

Table 4.1. Magnetic field amplitude and frequency ranges that can be used in the magneTherm

Coil turns	Capacitor type	Nominal frequency (kHz)	DC Power Supply voltage	DC Power Supply Current	Maximum Current (mT)
9	200 nF	164.2	22.6	25	23
9	88 nF	246.0	25.8	22.5	20
9	26 nF	412.6	28.9	19.6	16
9	15 nF	582.3	32.3	18.0	14
9	6.2 nF	942.1	32.6	14.5	12
17	200 nF	106.7	30	19.2	25
17	88 nF	160.2	25.8	13.5	17
17	26 nF	268.3	33.7	13.75	17
17	15 nF	378.8	37.3	12.8	16
17	6.2 nF	612	39.8	11.1	12

Briefly, 2 mL of samples with concentrations of 0.05 – 1.55 mg/mL is placed in a cryotube, which is enclosed in polystrene sample holder in order to prevent heat loss and placed in the induction coil that is cooled by using tap water. Fiberoptic probe (Osensa,Canada) is dipped into the sample and the local temperature enhancement is recorded at 1-second intervals in the presence of an externally applied magnetic field

(Figure 4.3). Before each measurement, the temperature of samples was stabilized and then alternating magnetic field (AMFs) was applied to nanofluids containing ferrimagnetic nanoparticles for at least 10 minutes at various frequencies (106.5kHz to 378.3kHz) and magnetic field strengths (12.8 to 20 kA/m).

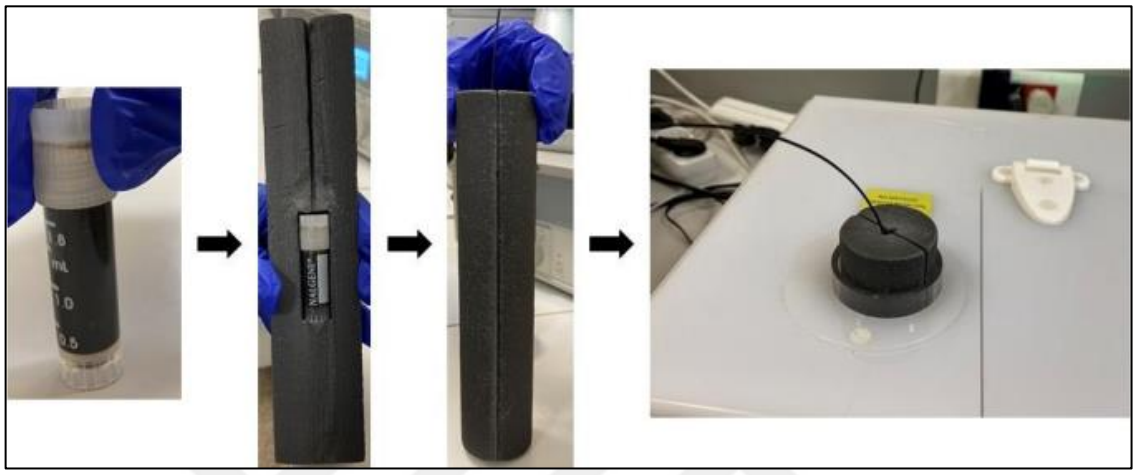

Figure 4.3. Preparation of samples to measure SAR on magneTherm

During the measurements, the temperature enhancement resulted from external alternating magnetic field were recorded by fiberoptic temperature sensor at 1-second intervals. The highest slope values (ΔT/Δt) of the obtained time dependent temperature change data were determined with Slope Analyzer package (OriginLab) (Figure 4.4). Prior to the calculation of maximum slopes, data has been smoothed by using Adjacent-Averaging method in order to remove the noise present in the temperature data. The slopes of the smoothed data were calculated via Slope Analyzer at 50-second intervals and the maximum slope (ΔT/Δt) was evaluated for each sample for the calculation of SAR. The spesific absorption rates (SAR) of water based ferrimagnetic magnetite nanoparticles were then calculated by using Equation 4.2.

$$SAR\ (\frac{W}{g}) = \frac{C.\rho}{\varphi}.\frac{\Delta T}{\Delta t} \tag{4.2}$$

where, ρ and C and is the density and specific heat capacity of water, respectively, φ is the concentration of magnetite based nanofluids in mg/mL, and $\Delta T/\Delta t$ represents the

maximum slope. Measurements were repeated up to 3 times and average SAR values were calculated in order to avoid any possible experimental error.

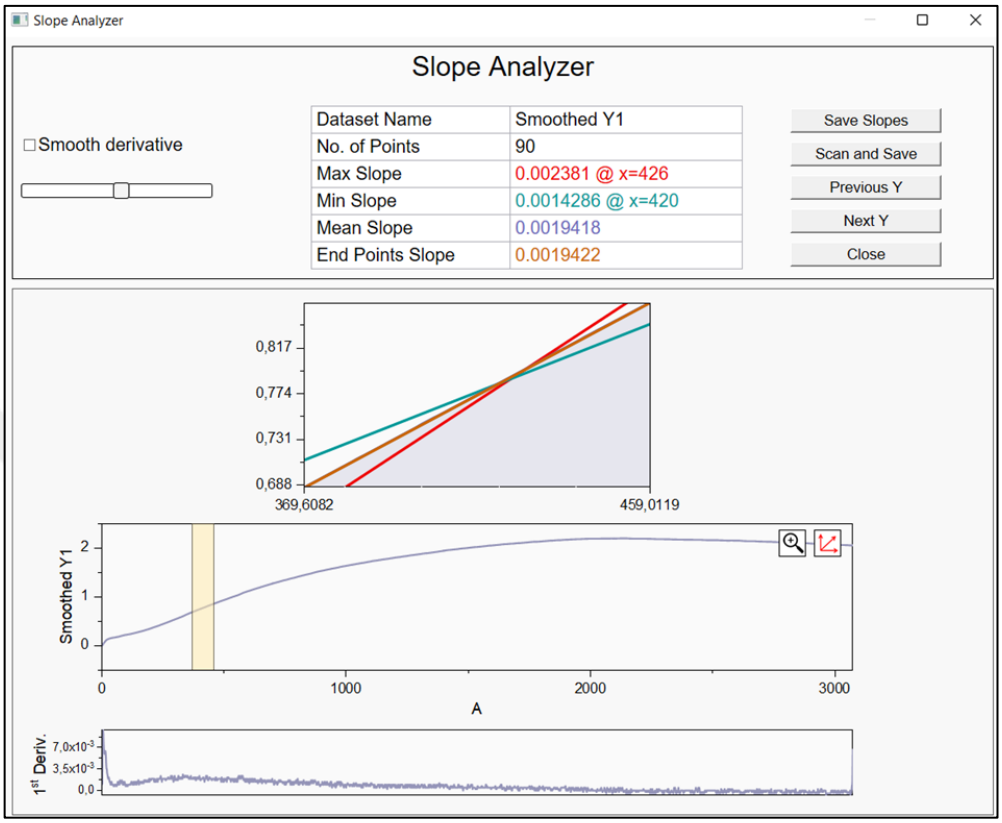

Figure 4.4. Determining maximum slope by using Slope Analyzer and OriginLab

4.4. HYPERTHERMIA TEST

The performance of DeNAno-MNP conjugates in magnetic hyperthermia was evaluated. Initially, Panc1 and Panc 02 cell lines were grown in appropriate mediums (DMEM High Glucose pyruvate (+) medium containing 10 percent FBS or 1 percent glutamax, 1 percent penicillin streptomycin at 37°C, in an incubator with 5 percent CO_2 air flow). Cells were then seeded at $5x10^4$ cells per well on a 12-well microplate and incubated at 37 °C for 24 hours. After 24 hours, the medium was incubated with MNP or DeNAno-MNP equivalent to 60 µg magnetite nanoparticles/mL. The medium was discarded and the cells in the wells were gently washed 2 times with PBS for removing MNP or DeNAno-MNPs that were not successfully attached to the cells. The cells were resuspended by being lifted from the surface by trypsin-EDTA and centrifuged at 1500 rpm/min at 4 °C. The

supernatant obtained after centrifugation was discarded and the precipitate containing the cells was resuspended in 2 ml of fresh medium. An alternating magnetic field at a frequency of 106.5 kHz and amplitude of 25 mT was applied to the suspended cells for 1 hour and the time-dependent temperature changes were monitored and recorded via the optical temperature sensor. Following the hyperthermia test, cell viability and cell death rates were determined. In addition to the magnetic field treated MNPs and DeNAno-MNP sample groups, a negative control group (untreated cells) and a positive control group (magnetic field applied cells without DeNAno-MNP) were also analyzed for comparison.

5. RESULTS AND DISCUSSION

5.1. CHARACTERIZATION OF MAGNETITE NANOPARTICLES

The average particle size and size distributions of PAA modified magnetite nanoparticles were determined from TEM images by measuring both the short and long axis of 100 individual nanoparticles. As seen in Figure 5.1, the average particle size of bare and PAA-coated nanoparticles were determined as 41.6±6.9 and 29.3±7.4 nm, respectively. These results demonstrated that PAA coating dramatically affected the average particle size of nanoparticles possibly due to the inhibition of particle growth stage. In addition, TEM analysis showed that the morpholoy of PAA modified nanoparticles were mainly spherical where as the bare nanoparticles exhibited well defined cubic and/or octahedral morphologies.

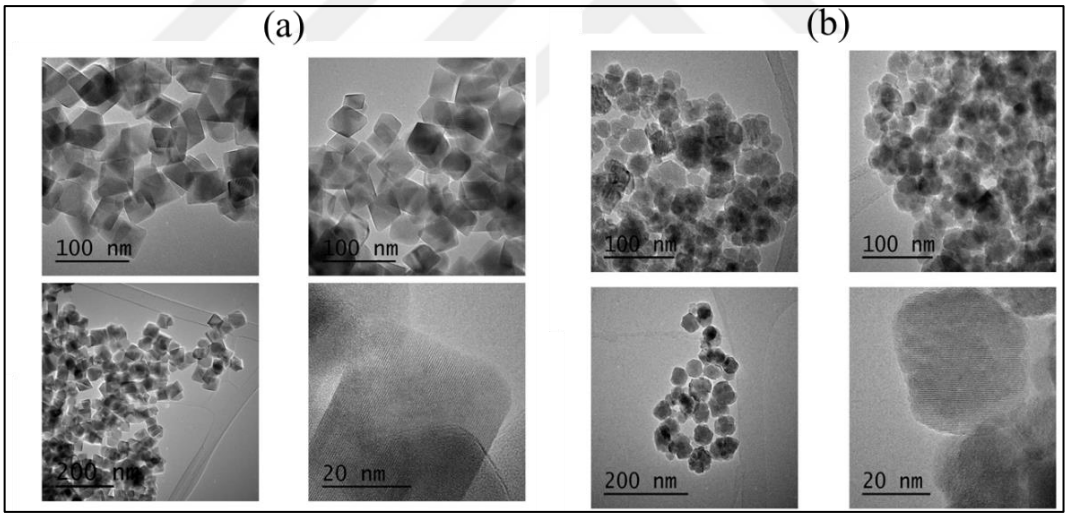

Figure 5.1. TEM analysis of ferrimagnetic magnetite nanoparticles obtained by partial oxidation method (a) bare (b) PAA modified

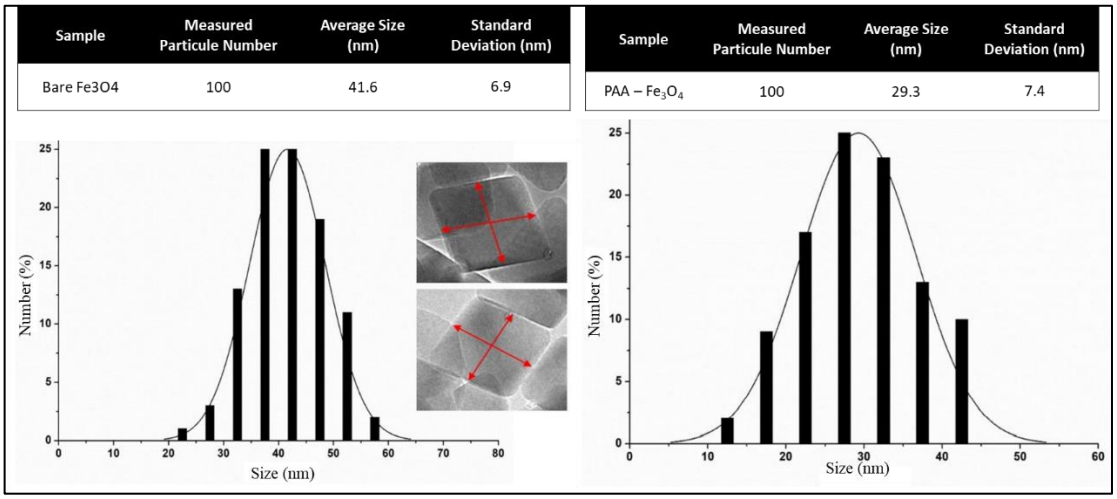

Figure 5.2. Size distribution histogram of bare and PAA coated magnetite nanoparticles synthesized via partial oxidation method

The size distribution of PAA coated and bare magnetite nanoparticles are represented in Figure 5.2, which can be observed that the particle distribution can be dramatically influenced by polymer addition during the nanoparticle synthesis. The crystalline phase of both coated and uncoated iron oxide nanoparticles was specified by powder X-Ray Diffraction (XRD) as shown in Figure 5.3. Results illustrated that the obtained nanoparticles were highly crystalline with cubic inverse spinel structure, and the relative intensity and position the reflection peaks confirmed the formation of magnetite (Fe_3O_4) phase and the absence of extra peaks indicated that no secondary phase or impurities existed within the sample.

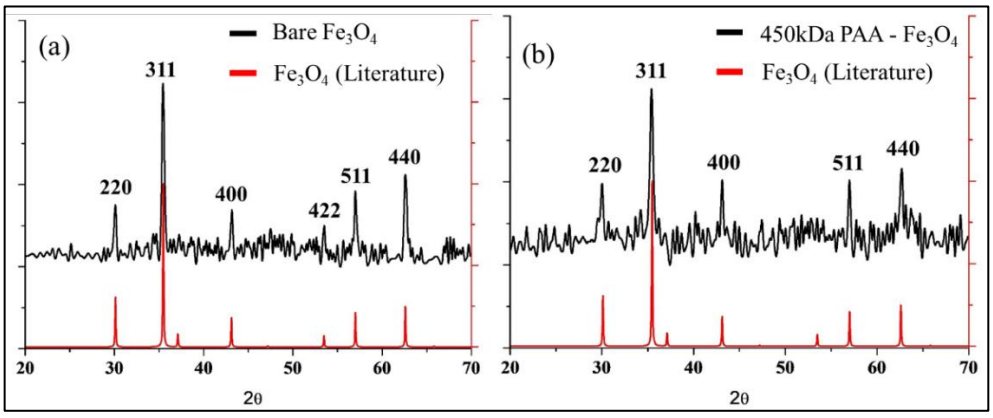

Figure 5.3. Comparison of the XRD patterns of (a) bare and (b) polymer functionalized nanoparticles with the literature values of magnetite

In addition, Selected Area Electron Diffraction (SAED) was conducted to verify the presence of magnetite phase as shown in Figure 5.4. The formation of highly crystalline magnetite phase can be verified by white spots/bright diffraction rings that can be assigned to corresponding lattice planes of magnetite. In addition, Figure 5.5 shows the high resolution TEM image of magnetite nanoparticles and FTT analysis.

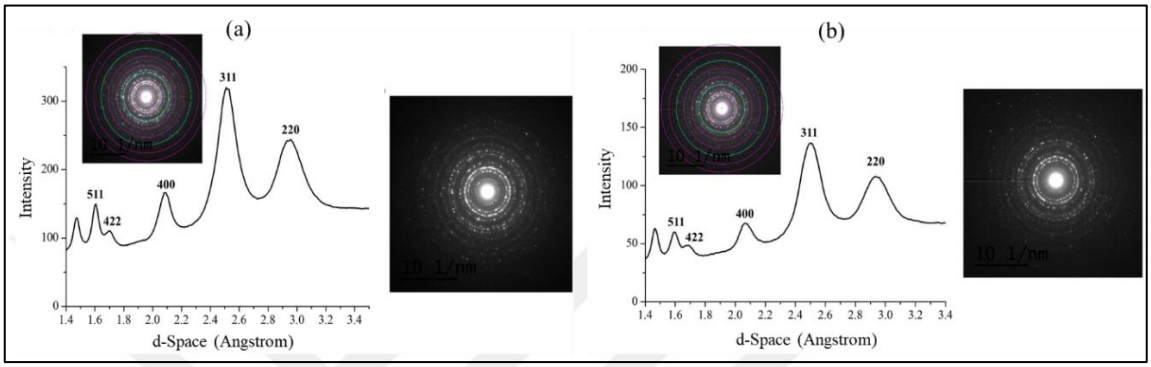

Figure 5.4. Selected area electron diffraction (SAED) of a) bare b) PAA (450kDa) functionalized magnetite nanoparticles

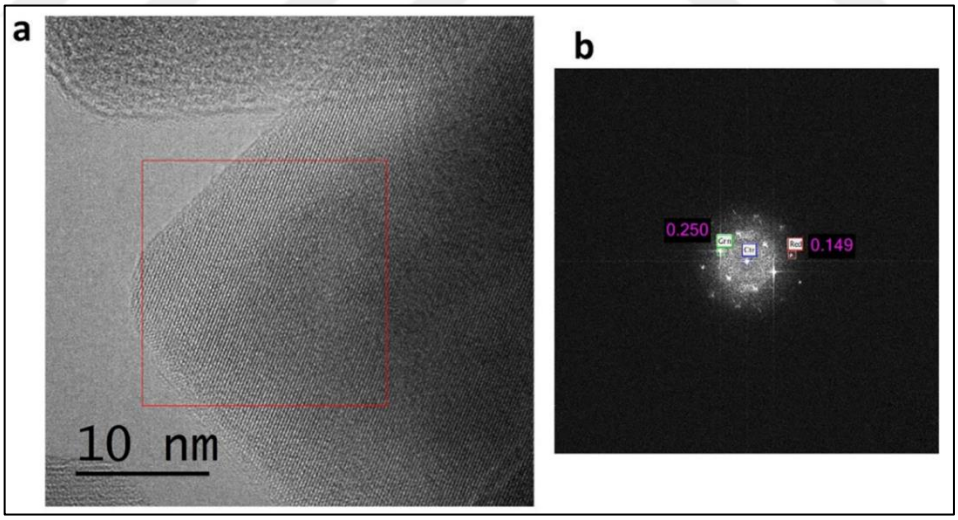

Figure 5.5. Determining d-space of mare magnetite nanoparticles a) TEM image b) FTT image

Thermogravimetric analysis (TGA) presented in Figure 5.6, which shows a 1 percent weight loss for bare magnetite nanoparticles resulting from the evaporation of physically adsorbed water from the surface of nanoparticles. In addition, PAA modified magnetite

nanoparticles exhibited a further loss of 4 wt. percent between 250 – 500°C, indicating the existence of a thermally degradable organic material (PAA) on the surface of magnetite nanoparticles. In addition, the degradation and onset temperature of polyacrylic acid shifted from 190 °C to 250 °C which is an indication for the strong interaction between the nanoparticle and PAA [65].

The magnetic properties of PAA modified magnetite nanoparticles were investigated by obtaining hysteresis loops via Vibrating Sample Magnetometer (VSM) (Figure 5.7). Magnetite nanoparticles functionalized with PAA (450kDa) were found to present a saturation magnetization (M_s) around 55 emu/g which is considerably much higher than nanoparticles synthesized via conventional co-precipitation method that is able to produce superparamagnetic nanoparticles. Moreover, the obtained nanoparticles exhibit ferrimagnetic properties as verified by the observation of coercivity and remanence on the magnetization loop.

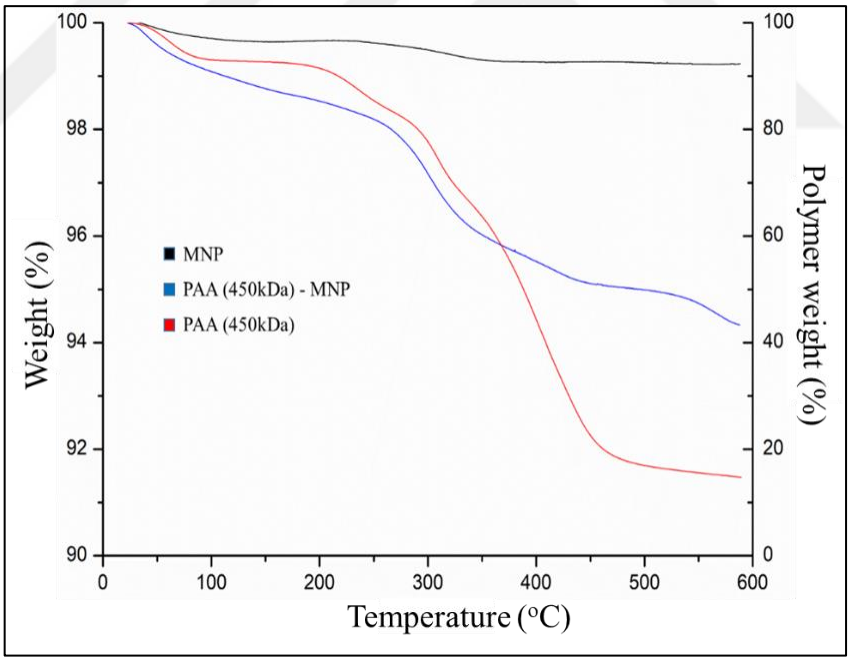

Figure 5.6. TGA curves for bare magnetite nanoparticles (MNP), PAA(450kDa) coated magnetite nanoparticles and PAA(450kDa)

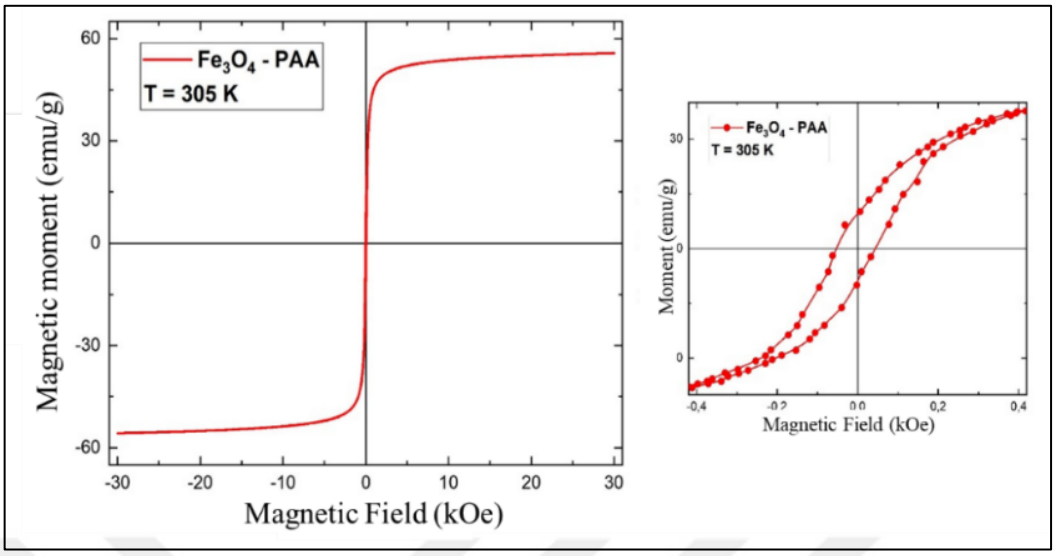

Figure 5.7. Vibrating sample magnetometer (VSM) analysis of funtionalized magnetite nanoparticles using PAA (450kDa)

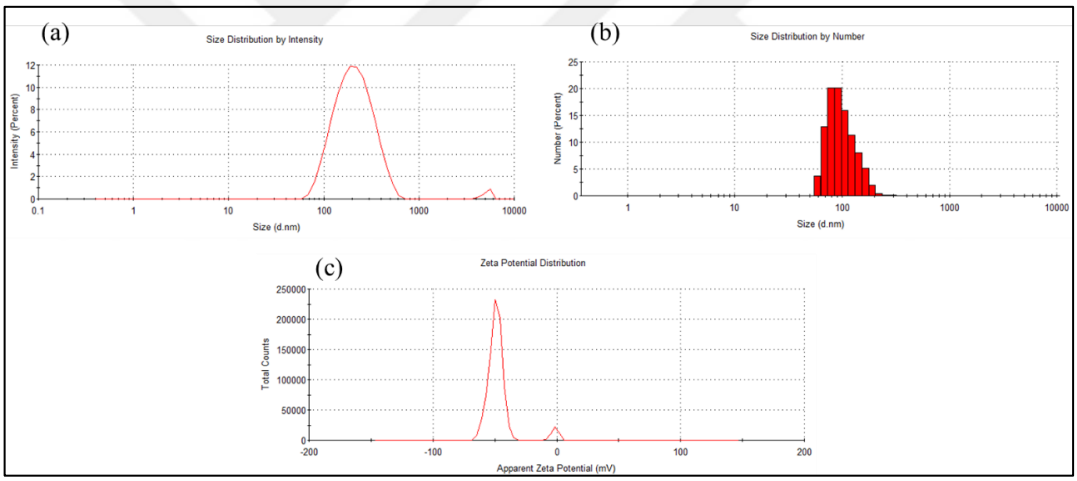

Figure 5.8. Dynamic Light Scattering (DLS) analysis of ferrimagnetic nanoparticles coated with PAA(450kDa) a) size distribution by intensity b) size distribution by number c) zeta potential

Dynamic light scattering (DLS) analysis of PAA (450kDa) and PAA (250kDa) modified magnetite nanoparticles are shown in Figure 5.8 and Figure 5.9, respectively. According to the results, it can be illustrated that the hydrodynamic diameter of ferrimagnetic nanoparticles coated with PAA (450kDa) and PAA (250kDa) are 175 and 143 nm, respectively. Moreover, number average hydrodynamic diameter of ferrimagnetic nanoparticles are measured as 91.3 and 68.1 nm, which is considerably higher than the

diameter obtained from TEM analysis that can be attributed to the existence of polymer on the surface of magnetite nanoparticles. Moreover, the zeta potential of nanoparticles were measured as -47.3 mV and -56 mV respectively possibly due to the presence of carboxyl groups of PAA on the surface of nanoparticles leading to colloidal stabilization via strong electrostatic repulsion.

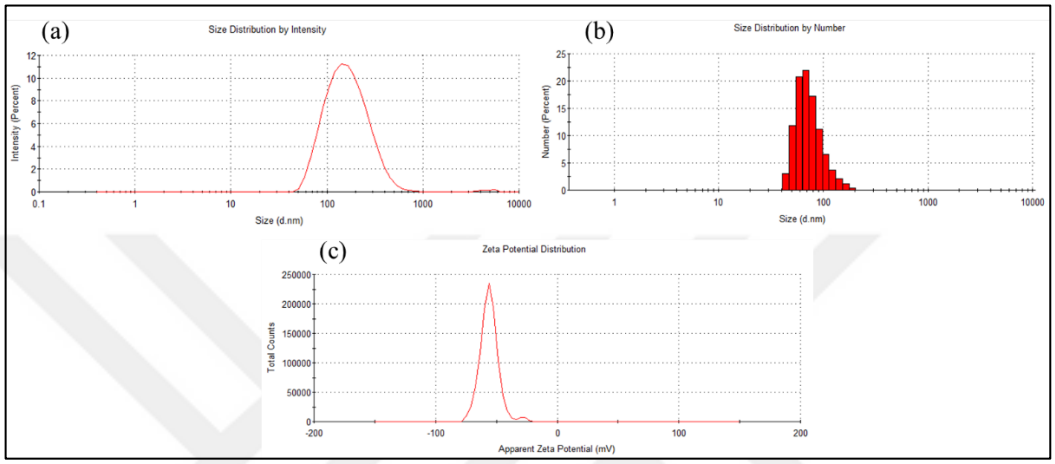

Figure 5.9. Dynamic Light Scattering (DLS) analysis of ferrimagnetic nanoparticles coated with PAA (250kDa) a) size distribution by intensity b) size distribution by number c) zeta potential

5.2. SPECIFIC ABSORPTION RATE (SAR) OF MAGNETITE NANOPARTICLES

In order to reveal the performance of ferrimagnetic magnetite nanoparticles synthesized via partial oxidation method in hyperthermia applications, SAR measurement of both bare and functionalized particles were conducted in the presence of an externally applied magnetic field as a function of concentration, magnetic field strength and frequency. Due to lack of non-magnetic layer on the surface, the magnetic properties of bare nanoparticles are much higher than functionalized particles. As represented in Figure 5.10, a temperature increase of almost 25 ^{o}C was recorded for bare magnetite nanoparticles under a frequency of 106.7 kHz and a magnetic amplitude of 25 mT. Although this remarkable enhancement in the temperature is desirable for hyperthermia, the lack of colloidal

stability of bare magnetite nanoparticles makes them unsuitable for biomedical applications.

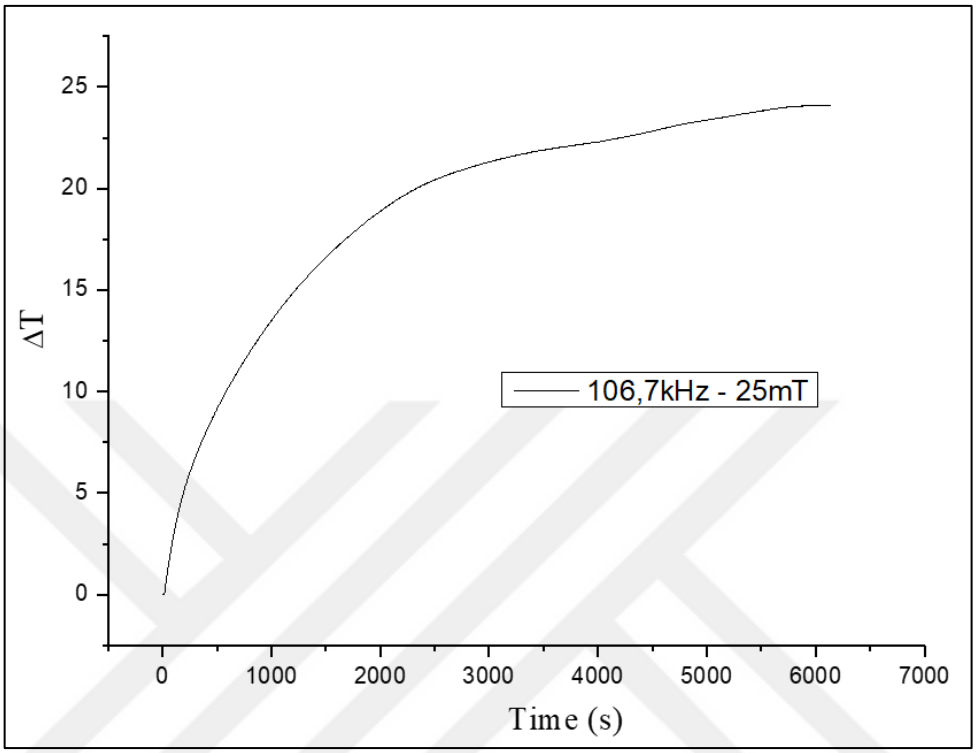

Figure 5.10. Time-dependent temperature change of bare Fe3O4 nanoparticles synthesized by partial oxdation method

Heat dissipation performance of nanofluids consisting of PAA modified ferrimagnetic magnetite nanoparticles was investigated at concentrations ranging from 0.05 to 1.55mg/mL for magnetic hyperthermia applications. Samples were exposed to externally applied alternating magnetic field with varying magnetic field amplitudes (H_0) and frequencies (f) and the corresponding temperature enhancements were recorded as a function of application time for the calculation of SAR.

5.2.1. Effect of Magnetic Field Amplitude and Frequency

The temperature enhancement of PAA (450kDa) modified magnetite nanofluids having different concentrations as a function of time is shown in Figure 5.11, under various magnetic field amplitudes (12.8 to 20 kA/m) while holding the frequency constant at

106,5 kHz. The results illustrated that increasing the magnetic field amplitude caused nanoparticles to generate more heat and enhanced temperature differences for each concentration of magnetite based nanofluids. Moreover, the local temperature was further enhanced with increasing concentration of ferrimagnetic nanoparticles. For the highest concentration of nanofluids (1.55 mg/ml) the local temperature was found to increase by almost 20 ^{o}C whereas for the lowest concentration (0.05 mg/ml) it is only measured as 2.5 ^{o}C at the same magnetic field strength and frequency. The faster heating profile of ferrimagnetic nanofluids with increasing concentration could be mainly ascribed to the enhanced relaxation due to the formation of large clusters/aggregates which affects the motion and rotation of nanoparticles under applied magnetic field [7,11].

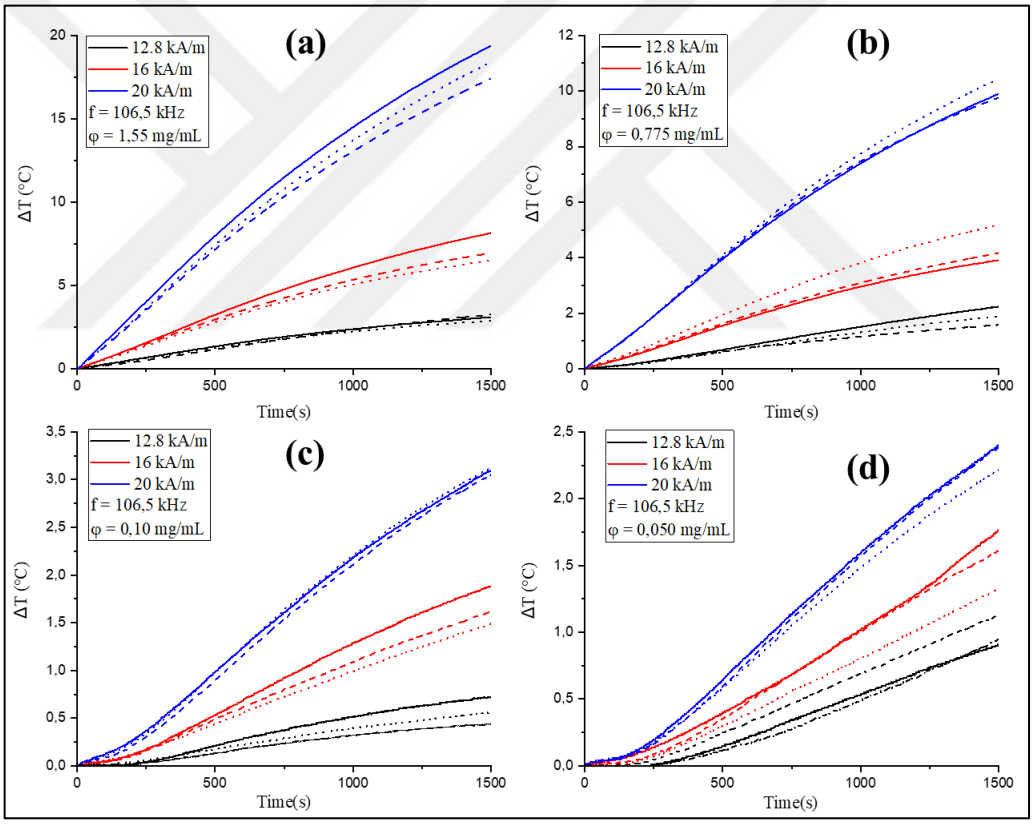

Figure 5.11. The effect of magnetic field amplitude over time-dependent temperature change of PAA (450 kDa) coated ferrimagnetic magnetite nanoparticles a) 1.55 mg/mL b) 0.775 mg/mL c) 0.10 mg/mL d) 0.05 mg/mL

In order to observe the effect of polymer molecular weight over the heating performance of nanofluids, PAA (250 kDa) coated magnetite nanoparticles at varying concentrations (0.05-1.55 mg/mL) were also exposed to externally applied alternating magnetic field with the amplitudes (H_0) in the range of 12.8 – 20 kA/m while holding the frequency constant at 106,5kHz. The effect of magnetic field amplitude at a fixed frequency over the temperature change of magnetite nanofluids are presented in Figure 5.12. Comparable results with PAA (450kDa) were also observed for PAA (250kDa) samples, such that an increase in the magnetic field strength concomitantly increases the local temperature change which additionally enhances with particle loading. The highest temperature change was obtained in ferrimagnetic magnetite nanofluid with a concentration of 1.55 mg/mL and at the maximum magnetic field amplitude of 20kA/m. Another important outcome is the effect of polymer weight on the heating profile of ferrimagnetic nanofluids. Results indicated that the ferrimagnetic magnetite nanoparticles functionalized with PAA (250kDa) exhibited lower heating capability than PAA (450kDa) modified alternatives which can be referred to the existance of a larger non-magnetic coating around the PAA (250kDa) modified particles as also supported by the zeta-potential measurements.

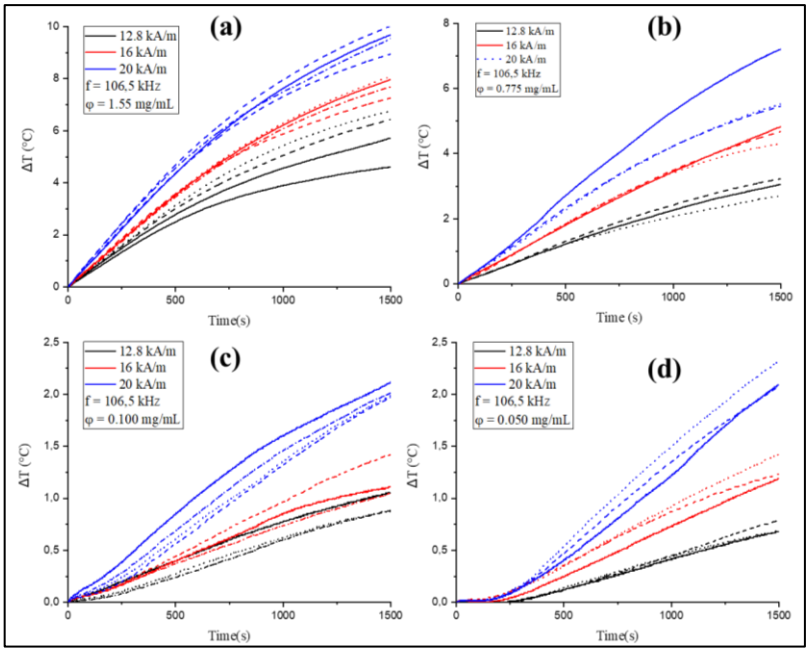

Figure 5.12. The effect of magnetic field amplitude over time-dependent temperature change of PAA (250 kDa) coated ferrimagnetic magnetite nanoparticles a) 1.55 mg/mL b) 0.775 mg/mL c) 0.10 mg/mL d) 0.05 mg/mL

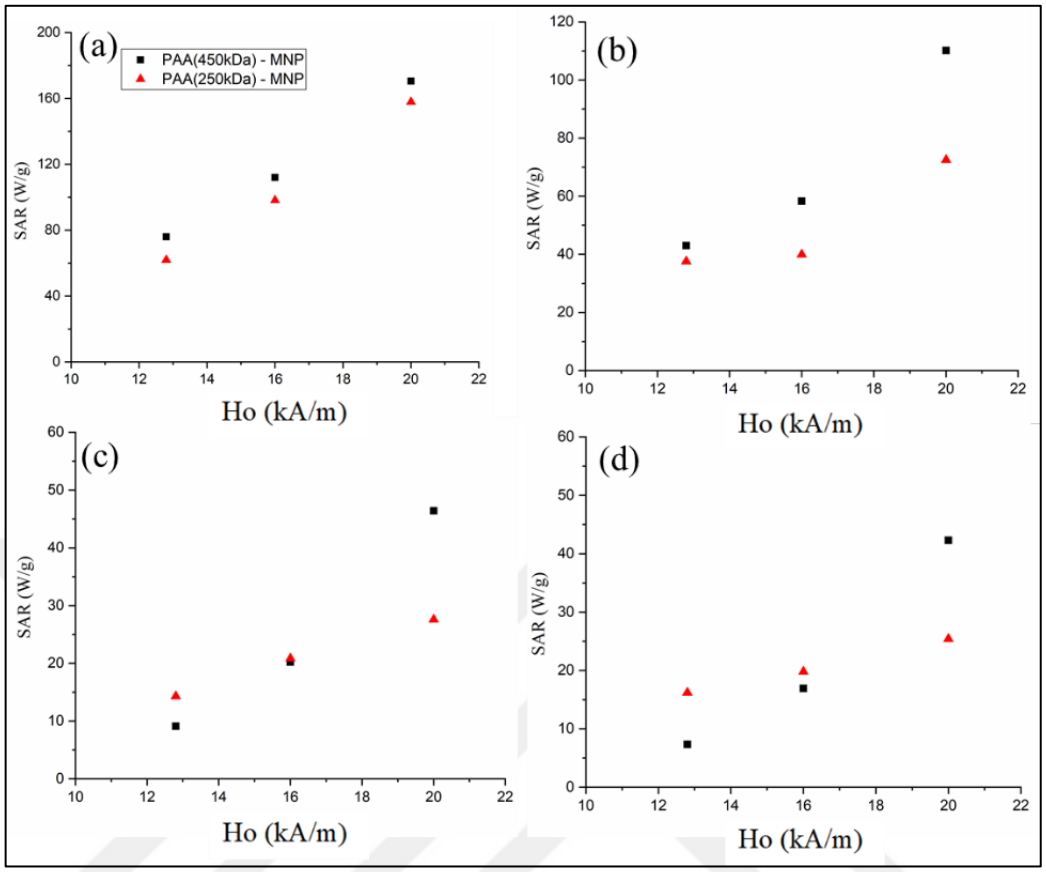

Figure 5.13. The effect of magnetic field amplitude (Ho) on the specific absorption rate (SAR) value of polymer coated ferrimagnetic magnetic nanofluids at a concentrations of (a) 0.05mg/mL,(b) 0.1mg/mL,(c) 0.775mg/mL (d) 1.55mg/mL

The effect of magnetic field strength over the SAR values of ferrimagnetic nanofluids consisting of PAA (250kDa) and PAA (450kDa) modified magnetite nanoparticles are presented in Figure 5.13. Results illustrated that SAR is enhanced with the increment of magnetic field amplitude, for each concentration of ferrimagnetic nanofluids at constant frequency as shown in the literature [5,11]. For instance, at a specific concentration of particles (0.05mg/mL), the SAR value of nanofluid consisting of PAA (450 kDa) and PAA (250 kDa) functionalized ferrimagnetic magnetite nanoparticles was increased from 76 to 170 W/g and 62 to 158 W/g respectively, as a consequence of magnetic field amplitude increment from 12.8 to 20.0kA/m. The obtained elevation in the SAR values can possibly be attributed to the shortening of Nèel relaxation time as a result of increasing magnetic field intensity [81].

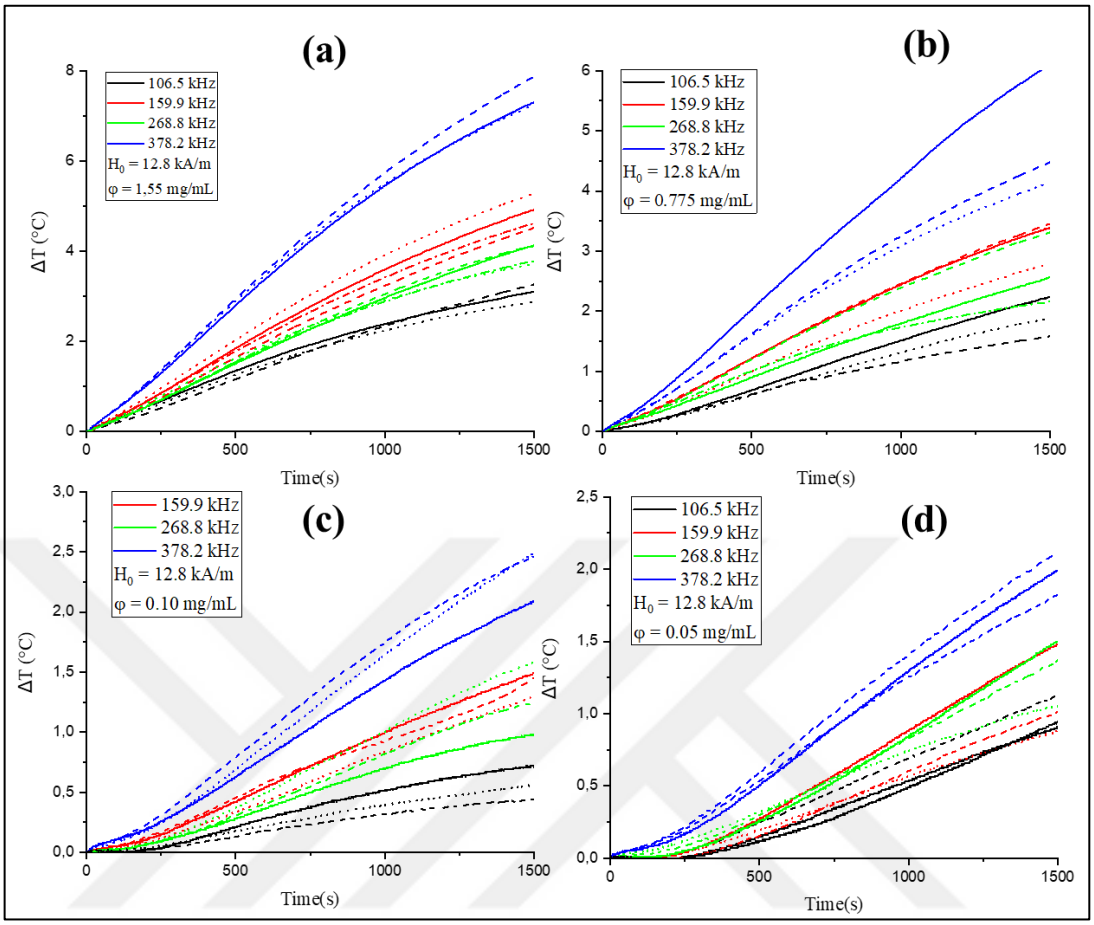

Figure 5.14. The effect of magnetic field frequency (f) over time-dependent temperature change of PAA (450 kDa) coated ferrimagnetic magnetite nanoparticles a) 1.55 mg/mL,b) 0.775 mg/mL,c) 0.10 mg/mL,d) 0.05 mg/mL

In order to investigate the significance of magnetic field frequency over the SAR of ferrimagnetic nanofluids, the calorimetric measurements were performed at a field amplitude of 12.8kA/m, while the frequency was altered from 106,5 to 378,3kHz. Figure 5.14 shows the temperature change of ferrimagnetic nanofluids consisting of PAA (450kDa) modified magnetite nanoparticles at various concentrations, as a function of magneitc field frequency. According to the results, it was observed that the temperature changes enhanced with an increase in magnetic field frequencies at a fixed magnetic field amplitude. Additionally, an increase in concentration of ferrimagnetic nanoparticles further augmented the temperature rise. The highest temperature increase up to 8 ^{o}C was obtained at a frequency of 378.8 kHz and for a concentration of 1.55 mg/mL, as expected. Similar results were obtained for PAA (250kDa) functionalized magnetite nanoparticles

and illustrated in Figure 5.15, which indicates an increase in both magnetic field frequency and particle loading enhance individually the local temperature change for ferrimagnetic magnetite containing nanofluids.

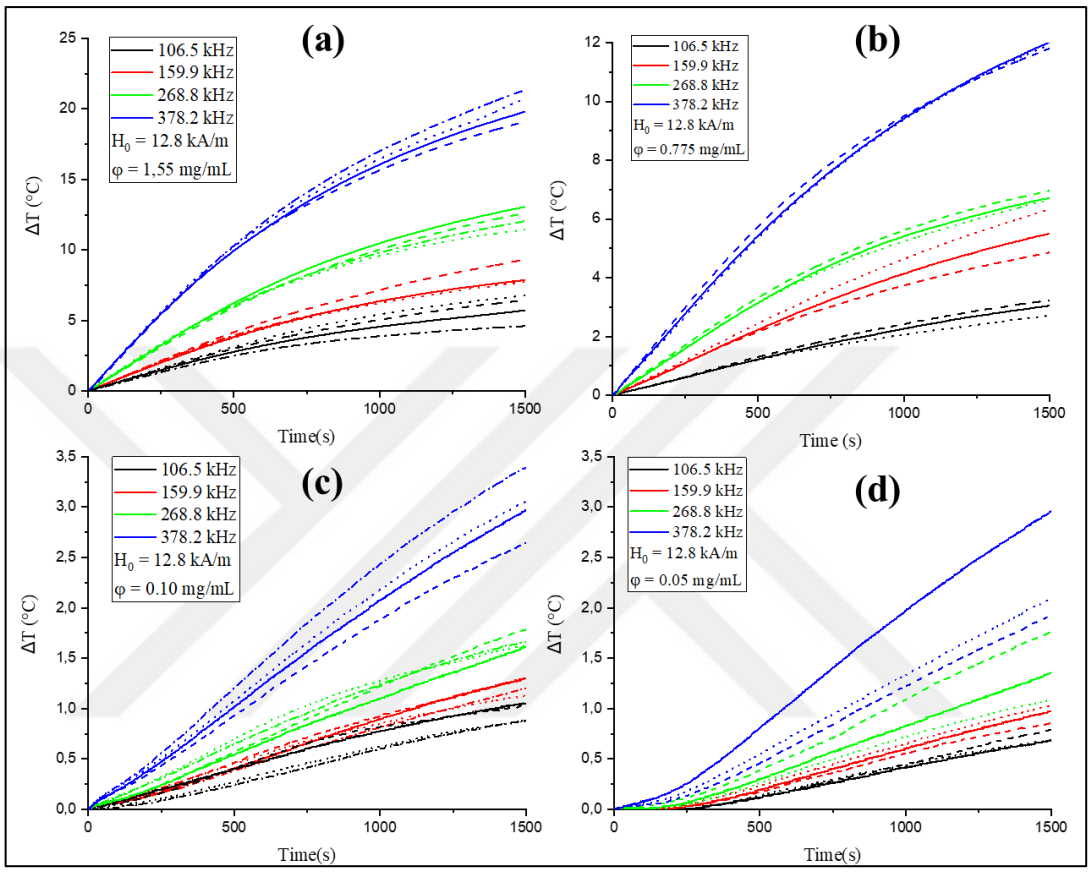

Figure 5.15. The effect of magnetic field frequency over time-dependent temperature change of PAA (250 kDa) coated ferrimagnetic magnetite nanoparticles a) 1.55 mg/mL b) 0.775 mg/mL,c) 0.10 mg/mL,d) 0.05 mg/mL

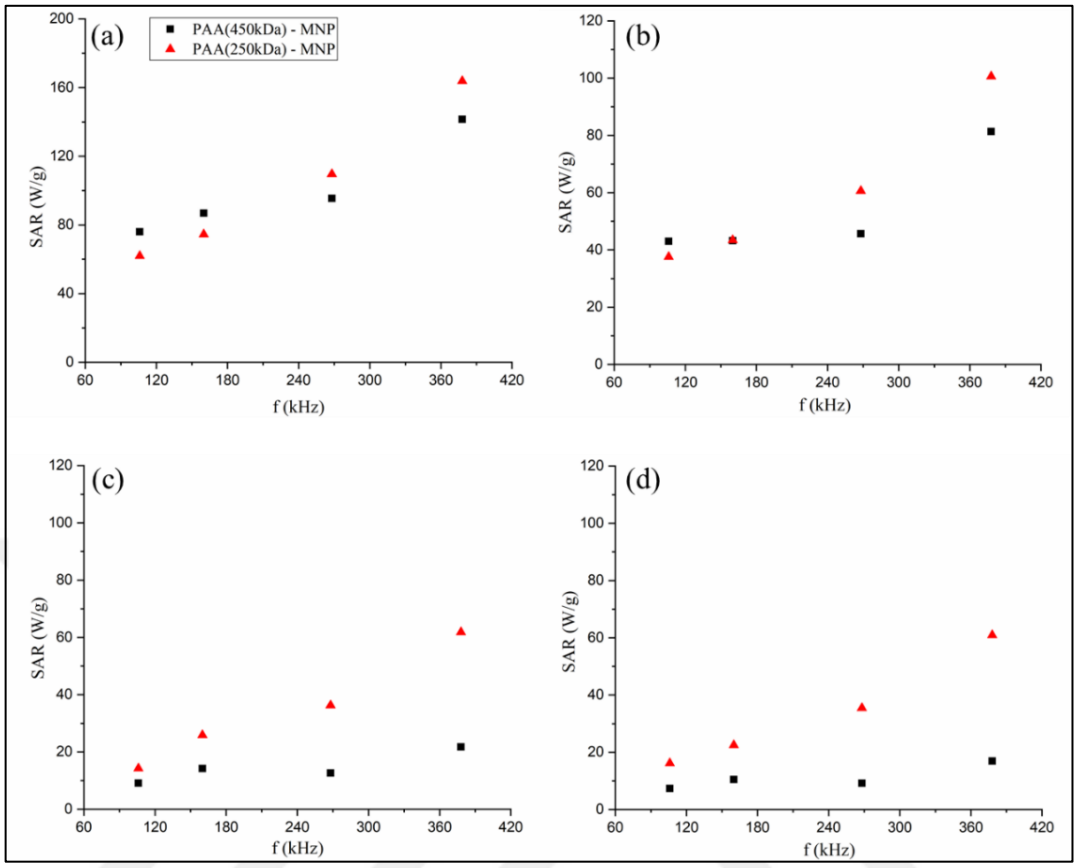

Figure 5.16. The effect of frequency (*f*) on the specific absorption rate (SAR) value of ferrimagnetic magnetic nanofluids at a concentrations of (a) 0.05mg/mL,(b) 0.1mg/mL,(c) 0.775mg/mL,(d) 1.55mg/mL

Figure 5.16 presents the calculated specific absorption rate of ferrimagnetic nanofluids at varying concentrations, as a function of applied field frequency. Higher SAR values were observed with increasing magnetic field frequencies regardless of concentration of nanoparticles as previously shown in the literature (5,11). For instance, at a concentration of 0.05mg/mL, the SAR of PAA (450kDa) modified magnetite nanoparticle based nanofluid was increased from 76 to 141 W/g as frequency was increased from 106.5 to 378.3 kHz while PAA (250 kDa) modified nanoparticles exhibited 61 to 164 W/g at the same frequency interval.

5.2.2. Concentration Effect

In order to investigate the influence of concentration of magnetite nanoparticles over the hyperthermia performance, measurements were performed under externally applied alternating magnetic field at a various magnetic field strengths (12,8 – 20.0 kA/m) and frequencies (106,5-378,2 kHz) for a concentration range from 0.05 to 1.55 mg/mL.

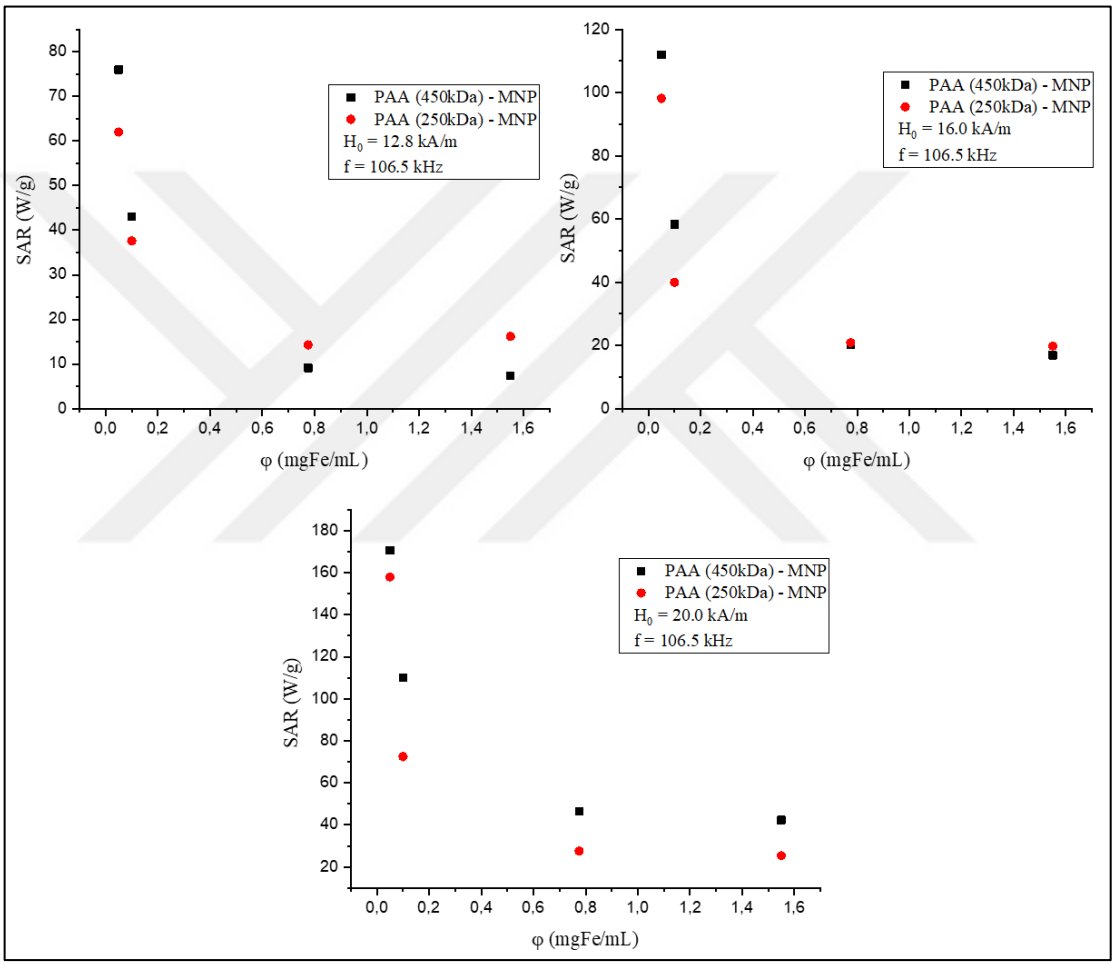

Figure 5.17. Effect of nanoparticle concentration over SAR values of ferrimagnetic nanofluids at different magnetic field amplitude (Ho)

While calculating the SAR value of magnetite nanoparticles, the maximum slopes of the time-dependent temperature change curves were calculated and substituted in Equation 4.2. The nature of Equation 4.2 and results illustrated in Figures 5.11, 5.12, 5.14 and 5.15, indicate that an increase in particle concentration also lead to an increase in local

temperature change, therefore SAR was initially expected to behave almost independent to particle concentration. However, according to results given in Figure 5.17, increasing the concentration of magnetite nanoparticles in the suspension lead to a deterioration in the specific absorption rate, even though significant temperature rise was observed with increasing amount of particle loading. For magnetic nanofluids consisting of both PAA (450 kDa) and PAA (250kDa) functionalized nanoparticles, a significant reduction on the heating power was observed as concentration increases. For instance, in the case of magnetic field amplitude of 12.8 kA/m and 106.5 kHz, the SAR value of PAA(450kDa)-MNP and PAA(250kDa)-MNP were dramatically reduced from 76 to 7 W/g and 62 to 16 W/g respectively by the increment in concentration from 0.05 to 1.55mg/mL (Figure 5.18). The highest SAR value was calculated as 169 W/g at 0.05 mg/mL concentration, under 20 kA/m magnetic field strength for PAA(450kDa) modified magnetite nanoparticles at the lowest concentration which is also promising for biomedical applications as this concentration is comparably low enough to be toxic. Results further indicated that at low concentration of nanoparticles, SAR values are very susceptive to a concentration change and highly affected by a variation in particle loading at dilute conditions however at higher concentrations the SAR values are nearly independent of concentration and remain almost constant.

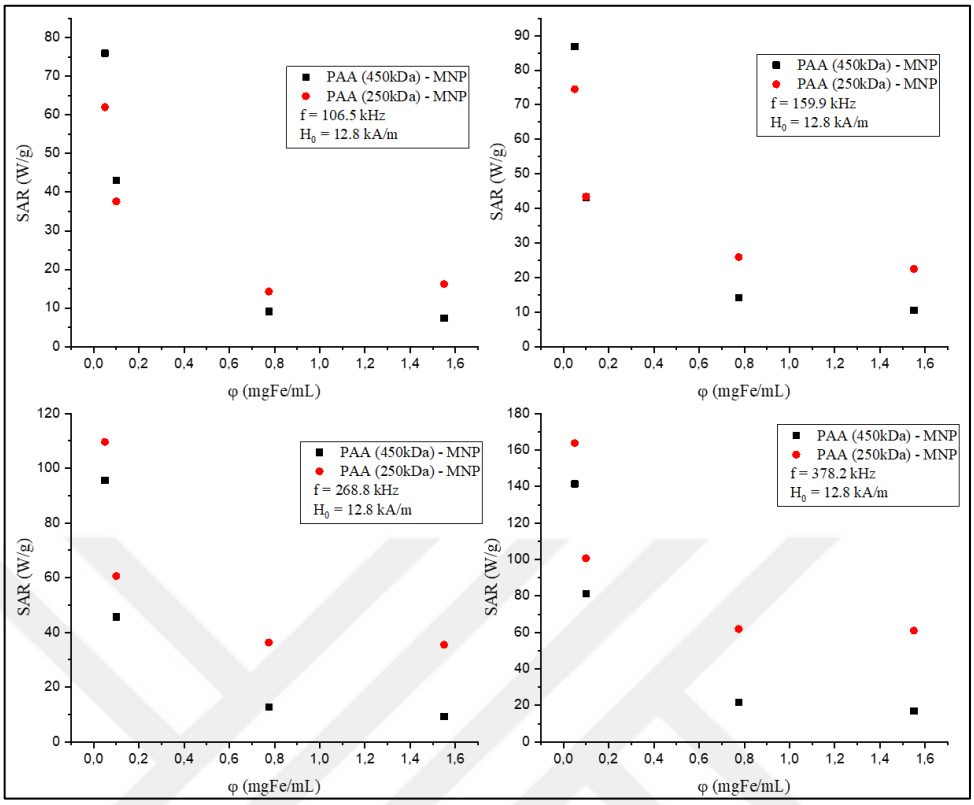

Figure 5.18. Effect of magnetic field frequency (*f*) over SAR values of ferrimagnetic nanofluids as a function of particle concentration

The influence of concentration of magnetite nanoparticles over SAR values were also investigated by performing measurements under various magnetic field frequencies (106.5 – 378,2 kHz) at a concentration range from 0.05 to 1.55 mg/mL. In parallel with previous results, a significant degradation on the hyperthermia performance of magnetite nanofluids were observed for both PAA (450 kDa) and PAA (250 kDa) modified nanoparticles as concentration increases. For instance, at a magnetic field strength and frequency of 12.8 kA/m and 159.9 kHz, the SAR value of PAA(450kDa)-MNP and PAA(250kDa)-MNP were dramatically reduced from 87 to 11 W/g and 75 to 22 W/g respectively by the increment in concentration from 0.05 to 1.55mg/mL. The highest SAR value was calculated as 164 W/g at the lowest concentration of 0.05 mg/mL for PAA (250 kDa) coated magnetite nanoparticles at a magnetic field frequency of 378.8 kHz.

The dynamic behaviour of SAR values can be attributed to the inter-particle dipole dipole interactions that are directly influenced by the nanoparticle concentration. It is clear that,

as the concentration of ferrimagnetic nanofluids increases, the mean distance between adjacent magnetic particles is reduced. Under the external magnetic field, since the particles get closer to each other as a consequence of an increase in particle concentration, dipolar magnetic moment interactions of particles are enhanced. Nèel relaxation, the internal rotation of the magnetic moment, is much more sensitive and strongly dependent to the dipole-dipole interaction rather than Brownian relaxation [82]. Thus, increasing the concentration of ferrimagnetic nanoparticles decreases susceptibility and Nèel relaxation time as a result of higher dipolar interactions, which may be significant reason for decreasing the SAR [10]. In other words, as the interaction between particles gets stronger, the hyperthermia performance of ferrimagnetic nanoparticles is weaken. On the other hand, the interparticle dipolar interaction is significantly reduced at very low particle concentrations, which may improve the hyperthermia efficiency of the particles and increases SAR as a consequence of isolated nanoparticles. Although there is an ongoing discussion in the literature about the effect of concentration on the hyperthermia capacity of magnetic nanoparticles, similar results were published. A recent study published by Tompinks et al [83] examined the effect of nanoparticle concentration over the induction heating response in the presence of an alternating magnetic field. The results indicated a consistent decrease in SAR as particle concentration increases. Redondo et al.[7] experimentally investigated the influence of concentration over SAR of magnetic nanoparticles and reported a remarkable decrease in SAR with increasing particle concentration that was referred to the enhancement of dipolar magnetic moment interaction that are proportional to the particle concentration. They also pointed out that in the case of bare magnetite nanoparticles, completely different behavior of SAR can be observed, notably, the SAR is directly proportional to the particle concentration. This behavior may be attributed to the heating for bare nanoparticles is mainly resulted from hysteresis loss, whereas for coated magnetite nanoparticles, Brownian and Neel relaxation mechanism are governing [84]. Effect of particle concentration over SAR have also been presented by Serantes et al [9]. and Urtizberea et al [10] and results shows that the hyperthermia performance of magnetic nanoparticles is deteriorated as a result of reduction in the static susceptibility with increasing dipolar interactions with particle concentration. However, there are also contradictory studies which indicates that the SAR is independent of or increase with the nanoparticle concentration [72]. Correlated to both

arguments, our results demonstrated that the SAR is not affected by the concentration of ferrimagnetic nanoparticles at relatively higher nanoparticle loading while it is significantly vary at diluted cases. These findings indicate the importance of concentration range of magnetic nanoparticles used in hyperthermia applications due to non-linear behavior of SAR. The experimental specific absorption rate data for both PAA (450kDa) and PAA (250kDa) coated ferrimagentic nanoparticles as a function of sample concentration and magnetic field parameters can be found in Table 5.1, 5.2, 5.3 and 5.4.

Table 5.1. Specific Absorption Rate (SAR) data of PAA (450kDa) coated ferrimagnetic nanoparticles as a function of sample concentration and magnetic field amplitude

Sample Concentration (mg/mL)	Magnetic Field Amplitude (kA/m)	Magnetic Field Frequency (kHz)	SAR (W/g)	Standard Deviation
0.05	12	106.5	76.0	± 2.1
	16		112.0	± 13.3
	20		170.5	± 4.4
0.1	12	106.5	43.0	± 8.0
	16		58.3	± 7.9
	20		19.9	± 3.8
0.775	12	106.5	9.1	± 0.6
	16		20.2	± 2.5
	20		20.9	±1.6
1.55	12	106.5	7.3	± 0.2
	16		16.2	± 1.3
	20		16.9	± 1.7

Table 5.2. Specific Absorption Rate (SAR) data of PAA (450kDa) coated ferrimagnetic nanoparticles as a function of sample concentration and magnetic field frequency

Sample Concentration (mg/mL)	Magnetic Field Amplitude (kA/m)	Magnetic Field Frequency (kHz)	SAR (W/g)	Standard Deviation
0.05	12	106.5	76.0	± 2.1
		159.9	86.9	± 22.4
		268.8	95.5	± 15.5
		378.2	141.5	± 8.5
0.1	12	106.5	43.0	±8.0
		159.9	43.2	± 11.2
		268.8	45.7	± 8.2
		378.2	81.3	±7.7
0.775	12	106.5	9.1	±0.6
		159.9	14.2	±1.1
		268.8	12.6	±2.3
		378.2	21.7	±3.1
1.55	12	106.5	7.3	± 0.2
		159.9	10.5	± 0.9
		268.8	9.2	± 0.5
		378.2	16.9	± 0.4

Table 5.3. Specific Absorption Rate (SAR) data of PAA (250kDa) coated ferrimagnetic nanoparticles as a function of sample concentration and magnetic field amplitude

Sample Concentration (mg/mL)	Magnetic Field Amplitude (kA/m)	Magnetic Field Frequency (kHz)	SAR (W/g)	Standard Deviation
0.05	12	106.5	62.0	± 6.1
	16		98.2	± 26.0
	20		157.9	± 17.0
0.1	12	106.5	37.6	±7.5
	16		39.9	±6.4
	20		72.5	±7.3
0.775	12	106.5	14.3	±0.6
	16		20.9	±0.8
	20		27.6	±2.5
1.55	12	106.5	16.2	±1.2
	16		19.8	±0.4
	20		25.4	±1.0

Table 5.4. Specific Absorption Rate (SAR) data of PAA (450kDa) coated ferrimagnetic nanoparticles as a function of sample concentration and magnetic field frequency

Sample Concentration (mg/mL)	Magnetic Field Amplitude (kA/m)	Magnetic Field Frequency (kHz)	SAR (W/g)	Standard Deviation
0.05	12	106.5	62.0	± 6.1
		159.9	74.5	± 2.4
		268.8	109.7	± 24.1
		378.2	163.8	± 40.1
0.1	12	106.5	37.6	±7.5
		159.9	43.2	±2.2
		268.8	45.7	±5.6
		378.2	81.3	±10.3
0.775	12	106.5	14.3	±0.6
		159.9	25.9	±1.6
		268.8	36.3	±1.5
		378.2	61.9	±2.9
1.55	12	106.5	16.2	±1.2
		159.9	22.5	± 1.2
		268.8	35.5	±1.3
		378.2	60.9	±1.1

5.2.3. Hyperthermia Test of DeNAno-MNP Conjugates and Cell Viability of Panc01 and Panc02

An alternating magnetic field with a magnetic field amplitude of 20 kA/m and a frequency of 106.5 kHz was applied for 1-hour to Panc01 and Panc02 cells incubated with magnetite conjugated DeNAno particulates. Following the hyperthermia test, the cells were subjected to cell viability analysis and cell death rates were determined. In addition to suspensions containing magnetite and DeNAno-MNP, negative control group (untreated cells) and positive control group (cells without MNP and DeNAno-MNP, but magnetic field applied) were also included in the analysis. As a consequence of the technical limitations of the magneTherm device, cells were suspended in PBS and analyzed via flow cytometry (Millipore-Guava Technologies) by using PI (propidium iodide) staining. It is aimed to obtain a statistical data by expressing cells with PI staining as dead and those without as viable. After the hyperthermia test, cell viability measurements were performed and given in Figure 5.19 and Figure 5.20. Corresponding values were also presented in Table 5.5.

Table 5.5. Cells viability measurements of hyperthermia treated Panc01 and Panc02 cells

Panc01 Cells	**Living Cells (%)**	**Death Cells (%)**
Negative Control Group	77	23
Positive Control Group	78.6	21.4
MNP Group	83.9	16.1
MNP-DeNAno Group	38.1	53.7
Panc02 Cells	**Living Cells (%)**	**Death Cells (%)**
Negative Control Group	78.7	21.3
Positive Control Group	83	17
MNP Group	89.4	10.6
MNP-DeNAno Group	74.2	25.8

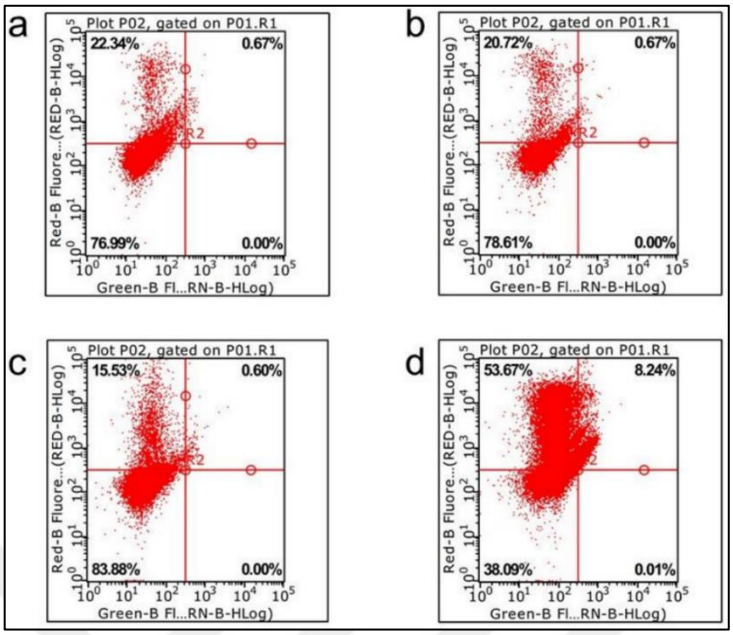

Figure 5.19. Cell viability test for Panc01 cells a) negative control b) positive control c) MNP treated group d) MNP-DeNAno treated group

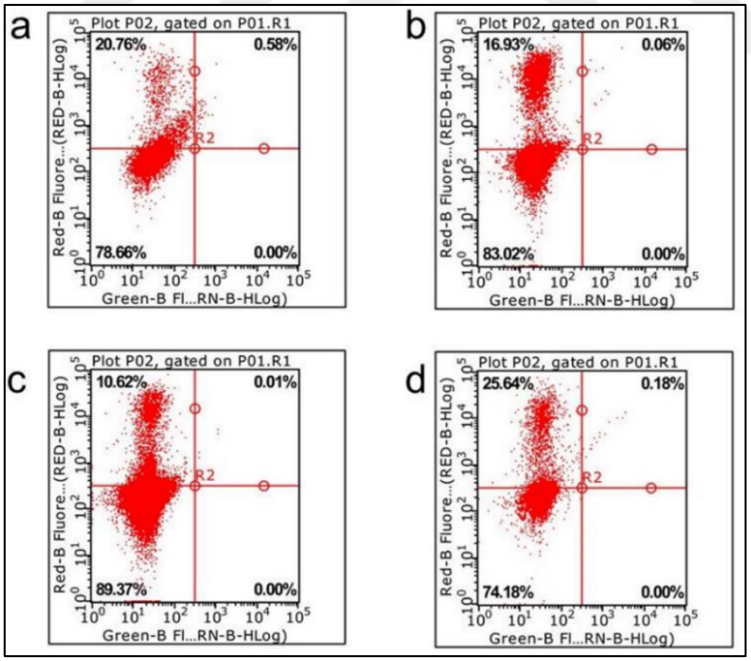

Figure 5.20. Cell viability test for Panc02 cells a) negative control b) positive control c) MNP treated group d) MNP-DeNAno treated group

The essential aim of applying PI staining to cells after hyperthermia test is the capability of designating affected cells as those will be stained with PI as a consequence of cell membrane damage which allow permeability. The results obtained and illustrated in Figure 5.19 and 5.20 indicated that magnetite nanoparticles conjugated DeNAno particulates adversely affect the viability of both Panc01 and Panc02 cell lines where the viability is relatively lower for Panc01 case. These results indicate the possible application of magnetite conjugated DeNAno particulates for efective hyperthermia applications where magnetite acts as heating sources while DeNAno serves as a recognition tool due to its explicit specifity to pancreatic cancer cell lines.

6. CONCLUSION

Numerous amount of extensive studies have been conducted for alternative cancer treatment methods as none of the existing conventional therapeutic approaches offer efficient treatment and total recovery. It should also be noted that cancer cells evolve and progress over time which results in new mutations and consequently making cancer treatment even more challenging. All of these conventinal methods for cancer treatment is performed at tissue and organ size scales, however killing and controlling tumors at cellular level is critical. Thus, more localized treatment methods have to be designed by considering target specific agents or ligands that can be able to identify and selectively attach to tumor cells while unaffecting healthy cells or tissues.

In this experimental study, the main goal is to conjugate biocompatible polyacrylic acid coated ferrimagnetic nanoparticles synthesized via partial oxidation technique with a DNA sequence (DeNAno) that can specifically attach to pancreatic cancer cell for possible magnetic hyperthermia applications in which magnetite serves as a heating source and DeNAno acts as recognition tool. The specific absorption rate (SAR) of both bare and surface functionalized nanoparticles were measured in order to demonstrate their suitability in magnetic hyperthermia applications. Later on the binding characteristics and affinities of the DeNAno conjugated magnetite nanoparticles to specific cancer cell lines were investigated in-vitro along with their cytotoxic and cell destruction effects caused by magnetic hyperthermia.

The hyperthermia performance of obtained ferrimagnetic nanoparticles were investigated by considering the effects of magnetic field strength, frequency and concetration of magnetite nanoparticles. An external alternating magnetic field were applied to ferrimagnetic nanofluids for specified time intervals at varying amplitudes (12.8 to 20.0 kA/m) and frequencies (106,5 to 378,3kHz). Futhermore, the nanoparticle concentration was altered within the range of 0.05 to 1.55mg/mL in order to observe the effect of particle loading on SAR. The effect of polymer molecular weight was also evaluated by comparing the SAR values of 250kDa and 450kDa polyacrylic acid modified magnetite nanoparticles.

According to the experimental results, for both 250kDa and 450kDa polyacrylic acid modified nanoparticles, the SAR values were enhanced by an increase in the magnetic field intensity regardless of concentration of nanoparticles. This increment in the SAR values were attributed to the shortening of Nèel relaxation time as a consequence of an increase in the magnetic field. Similar results were also obtained by considering the effect of magnetic field frequency where higher SAR values were recorded as applied field frequencies were increased at any particle loadings.

The specific absorption rate (SAR) as a function of ferrimagnetic magnetite nanoparticle concentration was also investigated and the results illustrated that the heating performance was dramatically reduced as the concentration of nanoparticles was increased. For both 250kDa and 450kDa functionalized ferrimagnetic nanoparticles, lower SAR values were obtained with increasing particle loading. Inter-particle dipole dipole interaction was suggested as the main mechanism for SAR dependency on particle concentration since the particles congregate at higher concentrations resulting in enhanced dipolar interactions which may influence the heating ability of particles and leading to a decrease in SAR.

Finally, the hyperthermia test was employed on pancreatic cancer cell lines, Panc01 and Pan02, which were incubated with magnetite conjugated DeNAno particulates and the results illustrated that cell lines were adversely affected by the hyperthermia application in the presence of DeNAno-MNP conjugates. All these outcomes demonstrate the possibility of combined practice of DeNAno particulates as successfull alternatives to aptamers and target specific ligands for their avidity on cancer cells and ferrimagnetic magnetite nanoparticles as heating sources due to their adequate SAR values even at low concentrations for magnetic hyperthermia applications.

REFERENCES

1. Cancer Research UK. Incidence @ Www.Cancerresearchuk.Org [Internet]. 2018. Available from: https://www.cancerresearchuk.org/health-professional/cancer-statistics/statistics-by-cancer-type/leukaemia-all/incidence

2. Institute NC. What-Is-Cancer @ Www.Cancer.Gov [Internet]. 2015. Available from: http://www.cancer.gov/cancertopics/what-is-cancer

3. Bucak S, Altan CL. Magnetic nanoparticles and cancer [Internet]. Nanotechnology in Cancer. Elsevier Inc.; 2017. 105–137 p. Available from: http://dx.doi.org/10.1016/B978-0-323-39080-4.00006-9

4. Ghosh R, Pradhan L, Devi YP, Meena SS, Tewari R, Kumar A, et al. Induction heating studies of Fe3O4 magnetic nanoparticles capped with oleic acid and polyethylene glycol for hyperthermia. J Mater Chem. 2011;21(35):13388–98.

5. Shah RR, Davis TP, Glover AL, Nikles DE, Brazel CS. Impact of magnetic field parameters and iron oxide nanoparticle properties on heat generation for use in magnetic hyperthermia. J Magn Magn Mater [Internet]. 2015;387:96–106. Available from: http://dx.doi.org/10.1016/j.jmmm.2015.03.085

6. Bakoglidis KD, Simeonidis K, Sakellari D, Stefanou G, Angelakeris M. Size-dependent mechanisms in AC magnetic hyperthermia response of iron-oxide nanoparticles. IEEE Trans Magn. 2012;48(4):1320–3.

7. Piñeiro-Redondo Y, Bañobre-López M, Pardiñas-Blanco I, Goya G, López-Quintela MA, Rivas J. The influence of colloidal parameters on the specific power absorption of PAA-coated magnetite nanoparticles. Nanoscale Res Lett. 2011;6:1–7.

8. Gonzales-Weimuller M, Zeisberger M, Krishnan KM. Size-dependant heating rates of iron oxide nanoparticles for magnetic fluid hyperthermia. J Magn Magn Mater. 2009;321(13):1947–50.

9. Serantes D, Baldomir D, Martinez-Boubeta C, Simeonidis K, Angelakeris M,

Natividad E, et al. Influence of dipolar interactions on hyperthermia properties of ferromagnetic particles. J Appl Phys. 2010;108(7).

10. Urtizberea A, Natividad E, Arizaga A, Castro M, Mediano A. Specific absorption rates and magnetic properties of ferrofluids with interaction effects at low concentrations. J Phys Chem C. 2010;114(11):4916–22.

11. Deatsch AE, Evans BA. Heating efficiency in magnetic nanoparticle hyperthermia. J Magn Magn Mater. 2014;354:163–72.

12. Huang HS, Hainfeld JF. IJN-43770-intravenous-magnetic-nanoparticle-hyperthermia. Int J Nanomedicine [Internet]. 2013;8:2521–32. Available from: https://www.ncbi.nlm.nih.gov/pmc/articles/PMC3720579/pdf/ijn-8-2521.pdf

13. Shi J, Xiao Z, Kamaly N, Farokhzad OC. Self-assembled targeted nanoparticles: Evolution of technologies and bench to bedside translation. Acc Chem Res. 2011;44(10):1123–34.

14. Farokhzad OC, Langer R. Impact of Nanotechnology on Hair Attributes. ACS Nano. 2009;3(1):1–7.

15. Sharma SK. Complex magnetic nanostructures: Synthesis, assembly and applications. Complex Magnetic Nanostructures: Synthesis, Assembly and Applications. 2017. 1–464 p.

16. Steiner JM, Sartor M, Sanchez AB, Messmer D, Freed A, Esener S, et al. DeNAno: Selectable deoxyribonucleic acid nanoparticle libraries. J Biotechnol. 2010;145(4):330–3.

17. Ruff LE, Marciniak JY, Sanchez AB, Esener SC, Messmer BT. Targeted and reversible cancer cell-binding DNA nanoparticles. Nanotechnol Rev. 2014;3(6):569–78.

18. cancer-cells-vs-normal-cells-2248794 @ www.verywellhealth.com [Internet]. Available from: https://www.verywellhealth.com/cancer-cells-vs-normal-cells-2248794

19. Bidram E, Esmaeili Y, Ranji-Burachaloo H, Al-Zaubai N, Zarrabi A, Stewart A, et al. A concise review on cancer treatment methods and delivery systems. J Drug Deliv Sci Technol [Internet]. 2019;54(July):101350. Available from: https://doi.org/10.1016/j.jddst.2019.101350

20. Moss RW. No Title. Brooklyn, NY : Equinox Press. 1995.

21. Damyanov CA, Maslev IK, Pavlov VS. Conventional Treatment of Cancer Realities and Problems. Ann Complement Altern Med. 2018;1(1):1–9.

22. Goldstein MR, Mascitelli L. Surgery and cancer promotion: Are we trading beauty for cancer? Qjm. 2011;104(9):811–5.

23. Mokhtari RB, Homayouni TS, Baluch N, Morgatskaya E, Kumar S, Das B, et al. Combination therapy in combating cancer SYSTEMATIC REVIEW: COMBINATION THERAPY IN COMBATING CANCER BACKGROUND. Oncotarget [Internet]. 2017;8(23):38022–43. Available from: www.impactjournals.com/oncotarget

24. Delbaldo C, Michiels S, Syz N, Soria, Jean-Charles Chevalier T Le, Pignon J-P. Benefits of Adding a Drug to a Single-Agent or a 2-Agent Chemotherapy Regimen in Advanced Non – Small-Cell Lung Cancer. Jama. 2004;292(4):470–84.

25. Oldham RK. Cancer Biotherapy: More Than Immunotherapy. Cancer Biother Radiopharm. 2017;32(4):111–4.

26. Akkın S, Varan G, Bilensoy E. A review on cancer immunotherapy and applications of nanotechnology to chemoimmunotherapy of different cancers. Molecules. 2021;26(11).

27. Old LJ. Cancer immunology. Sci Am. 1977;236(5):62–70, 72.

28. Rohaan MW, Wilgenhof S, Haanen JBAG. Adoptive cellular therapies: the current landscape. Virchows Arch. 2019;474(4):449–61.

29. Carter PJ, Senter PD. Antibody-drug conjugates for cancer therapy. Cancer J. 2008;14(3):154–69.

30. Belete TM. The current status of gene therapy for the treatment of cancer. Biol Targets Ther. 2021;15:67–77.

31. Das SK, Menezes ME, Bhatia S, Wang XY, Emdad L, Sarkar D, et al. Gene Therapies for Cancer: Strategies, Challenges and Successes. J Cell Physiol. 2015;230(2):259–71.

32. Lebedeva I V., Su ZZ, Sarkar D, Fisher PB. Restoring apoptosis as a strategy for cancer gene therapy: Focus on p53 and mda-7. Semin Cancer Biol. 2003;13(2):169–78.

33. Griffith T, Stokes B, Kucaba T, Earel Jr. J, VanOosten R, Brincks E, et al. TRAIL Gene Therapy: From Preclinical Development to Clinical Application. Curr Gene Ther. 2009;9(1):9–19.

34. Fisher PB, Sarkar D, Lebedeva I V., Emdad L, Gupta P, Sauane M, et al. Melanoma differentiation associated gene-7/interleukin-24 (mda-7/IL-24): Novel gene therapeutic for metastatic melanoma. Toxicol Appl Pharmacol. 2007;224(3):300–7.

35. Henriksson M, Luscher B. Proteins of the Myc network: Essential regulators of cell growth and differentiation. Adv Cancer Res. 1996;68:110–82.

36. Modok S, Mellor HR, Callaghan R. Modulation of multidrug resistance efflux pump activity to overcome chemoresistance in cancer. Curr Opin Pharmacol. 2006;6(4):350–4.

37. Pucci C, Martinelli C, Ciofani G. Innovative approaches for cancer treatment: Current perspectives and new challenges. Ecancermedicalscience. 2019;13:1–26.

38. Nguyen KT. Targeted nanoparticles for cancer therapy:Promises and challenges. J Nanomedicine Nanotechnol. 2011;2(5).

39. Pillai G. Nanotechnology Toward Treating Cancer [Internet]. Applications of Targeted Nano Drugs and Delivery Systems. Elsevier Inc.; 2019. 221–256 p. Available from: http://dx.doi.org/10.1016/B978-0-12-814029-1.00009-0

40. Awasthi R, Roseblade A, Hansbro PM, Rathbone MJ, Dua K, Bebawy M. Nanoparticles in Cancer Treatment: Opportunities and Obstacles. 2018;1696–709.

41. Panyam J, Labhasetwar V. B iodegradable nanoparticles for drug and gene delivery to cells and tissue. 2003;55:329–47.

42. Hematol J, Cheng Z, Li M, Dey R, Chen Y. Nanomaterials for cancer therapy : current progress and perspectives. J Hematol Oncol [Internet]. 2021;1–27. Available from: https://doi.org/10.1186/s13045-021-01096-0

43. Yao Y, Zhou Y, Liu L, Xu Y, Chen Q, Wang Y, et al. Nanoparticle-Based Drug Delivery in Cancer Therapy and Its Role in Overcoming Drug Resistance. 2020;7(August):1–14.

44. Tietze R, Lyer S, Dürr S, Struffert T, Engelhorn T, Schwarz M, et al. Efficient drug-delivery using magnetic nanoparticles - biodistribution and therapeutic effects in tumour bearing rabbits. Nanomedicine Nanotechnology, Biol Med [Internet]. 2013;9(7):961–71. Available from: http://dx.doi.org/10.1016/j.nano.2013.05.001

45. Attia MF, Anton N, Wallyn J, Omran Z, Vandamme TF. An overview of active and passive targeting strategies to improve the nanocarriers efficiency to tumour sites. J Pharm Pharmacol. 2019;71(8):1185–98.

46. Zhang L, Webster TJ, Zdrojewicz Z, Waracki M, Bugaj B, Pypno D, et al. Nanotechnology in therapeutics : a focus on nanoparticles as a drug delivery system R eview. Carbohydr Polym [Internet]. 2016;1(1):71–88. Available from: http://dx.doi.org/10.1016/j.nano.2010.07.004%5Cnhttp://linkinghub.elsevier.com/retrieve/pii/S1818087616300502%5Cnhttp://dx.doi.org/10.1016/j.carbpol.2016.06.026%5Cnhttp://www.cancerjournal.net/article.asp?issn=0973-1482%5Cnyear=2014%5Cnvolume=10%5Cnissue=

47. Ellington AD, Szostak JW. In vitro selection of RNA molecules that bind specific ligands. Nature. 1990;346(6287):818–22.

48. Mei L, Zhu G, Qiu L, Wu C, Chen H, Liang H, et al. Self-assembled

multifunctional DNA nanoflowers for the circumvention of multidrug resistance in targeted anticancer drug delivery. Nano Res. 2015;8(11):3447–60.

49. Kumar CSSR, Mohammad F. Magnetic nanomaterials for hyperthermia-based therapy and controlled drug delivery. Adv Drug Deliv Rev [Internet]. 2011;63(9):789–808. Available from: http://dx.doi.org/10.1016/j.addr.2011.03.008

50. Rajan A, Sahu NK. Review on magnetic nanoparticle-mediated hyperthermia for cancer therapy. J Nanoparticle Res. 2020;22(11).

51. Linh PH, Thach P Van, Tuan NA, Thuan NC, Manh DH, Phuc NX, et al. Magnetic fluid based on Fe3O4 nanoparticles: Preparation and hyperthermia application. J Phys Conf Ser. 2009;187.

52. Liu XL, Fan HM, Yi JB, Yang Y, Choo ESG, Xue JM, et al. Optimization of surface coating on Fe 3O 4 nanoparticles for high performance magnetic hyperthermia agents. J Mater Chem. 2012;22(17):8235–44.

53. Wildeboer RR, Southern P, Pankhurst QA. On the reliable measurement of specific absorption rates and intrinsic loss parameters in magnetic hyperthermia materials. J Phys D Appl Phys. 2014;47(49).

54. Brezovich IA, Atkinson WJ, Lilly MB. Local hyperthermia with interstitial techniques. Cancer Res. 1984;44(10 SUPPL.).

55. Kim DH, Kim KN, Kim KM, Lee YK. Targeting to carcinoma cells with chitosan- and starch-coated magnetic nanoparticles for magnetic hyperthermia. J Biomed Mater Res - Part A. 2009;88(1):1–11.

56. Kim MJ, Jang DH, Lee YI, Jung HS, Lee HJ, Choa YH. Preparation, characterization, cytotoxicity and drug release behavior of liposome-enveloped paclitaxel/Fe 3O 4 nanoparticles. J Nanosci Nanotechnol. 2011;11(1):889–93.

57. Hua MY, Yang HW, Chuang CK, Tsai RY, Chen WJ, Chuang KL, et al. Magnetic-nanoparticle-modified paclitaxel for targeted therapy for prostate cancer. Biomaterials [Internet]. 2010;31(28):7355–63. Available from:

http://dx.doi.org/10.1016/j.biomaterials.2010.05.061

58. Vilas-Boas V, Carvalho F, Espiña B. Magnetic hyperthermia for cancer treatment: Main parameters affecting the outcome of in vitro and in vivo studies. Molecules. 2020;25(12):1–30.

59. Manigandan A, Handi V, Sundaramoorthy NS, Dhandapani R, Radhakrishnan J, Sethuraman S, et al. Responsive Nanomicellar Theranostic Cages for Metastatic Breast Cancer. Bioconjug Chem. 2018;29(2):275–86.

60. Wang X, Yang R, Yuan C, An Y, Tang Q, Chen D. Preparation of Folic Acid-Targeted Temperature-Sensitive Magnetoliposomes and their Antitumor Effects In Vitro and In Vivo. Target Oncol. 2018;13(4):481–94.

61. Salunkhe AB, Khot VM, Pawar SH. Magnetic Hyperthermia with Magnetic Nanoparticles: A Status Review. Curr Top Med Chem. 2014;14(5):572–94.

62. Lenders JJM, Altan CL, Bomans PHH, Arakaki A, Bucak S, De With G, et al. A bioinspired coprecipitation method for the controlled synthesis of magnetite nanoparticles. Cryst Growth Des. 2014;14(11):5561–8.

63. Magnetite & Lodestone _ Mineral Photos, Uses, Properties.

64. Altan CL. Biomimetic synthesis, Magnetic Properties and Applications of MAgnetite Nanoparticles. 2014.

65. Altan CL, Gurten B, Sadza R, Yenigul E, Sommerdijk NAJM, Bucak S. Poly(acrylic acid)-directed synthesis of colloidally stable single domain magnetite nanoparticles via partial oxidation. J Magn Magn Mater [Internet]. 2016;416:366–72. Available from: http://dx.doi.org/10.1016/j.jmmm.2016.05.009

66. Sych ASO, Babutina AIT, Bykov TTO, Lobunets OOT. Effect of type and parameters of synthesis on the properties of magnetite nanoparticles. Appl Nanosci [Internet]. 2021;(0123456789). Available from: https://doi.org/10.1007/s13204-021-01797-5

67. Ortega G, Reguera E. Biomedical applications of magnetite nanoparticles

[Internet]. Materials for Biomedical Engineering: Nanomaterials-based Drug Delivery. Elsevier Inc.; 2019. 397–434 p. Available from: http://dx.doi.org/10.1016/B978-0-12-816913-1.00013-1

68. Reddy LH, Arias JL, Nicolas J, Couvreur P. Magnetic nanoparticles: Design and characterization, toxicity and biocompatibility, pharmaceutical and biomedical applications. Chem Rev. 2012;112(11):5818–78.

69. Voulgari E, Bakandritsos A, Galtsidis S, Zoumpourlis V, Burke BP, Clemente GS, et al. Synthesis, characterization and in vivo evaluation of a magnetic cisplatin delivery nanosystem based on PMAA-graft-PEG copolymers. J Control Release [Internet]. 2016;243:342–56. Available from: http://dx.doi.org/10.1016/j.jconrel.2016.10.021

70. Gautier J, Allard-Vannier E, Munnier E, Soucé M, Chourpa I. Recent advances in theranostic nanocarriers of doxorubicin based on iron oxide and gold nanoparticles. J Control Release [Internet]. 2013;169(1–2):48–61. Available from: http://dx.doi.org/10.1016/j.jconrel.2013.03.018

71. Sattarahmady N, Azarpira N, Hosseinpour A, Heli H, Zare T. Albumin coated arginine-capped magnetite nanoparticles as a paclitaxel vehicle: Physicochemical characterizations and in vitro evaluation. J Drug Deliv Sci Technol [Internet]. 2016;36:68–74. Available from: http://dx.doi.org/10.1016/j.jddst.2016.07.004

72. Parsian M, Unsoy G, Mutlu P, Yalcin S, Tezcaner A, Gunduz U. Loading of Gemcitabine on chitosan magnetic nanoparticles increases the anti-cancer efficacy of the drug. Eur J Pharmacol [Internet]. 2016;784:121–8. Available from: http://dx.doi.org/10.1016/j.ejphar.2016.05.016

73. Gunduz U, Keskin T, Tansik G, Mutlu P, Yalcin S, Unsoy G, et al. Idarubicin-loaded folic acid conjugated magnetic nanoparticles as a targetable drug delivery system for breast cancer. Biomed Pharmacother [Internet]. 2014;68(6):729–36. Available from: http://dx.doi.org/10.1016/j.biopha.2014.08.013

74. Asín L, Ibarra MR, Tres A, Goya GF. Controlled cell death by magnetic hyperthermia: Effects of exposure time, field amplitude, and nanoparticle

concentration. Pharm Res. 2012;29(5):1319–27.

75. Guardia P, Corato R Di, Lartigue L, Wilhelm C, Espinosa A, Garcia-hernandez M, et al. Guardia2012.Pdf. 2012;(4):3080–91.

76. Kim HC, Kim E, Jeong SW, Ha TL, Park SI, Lee SG, et al. Magnetic nanoparticle-conjugated polymeric micelles for combined hyperthermia and chemotherapy. Nanoscale. 2015;7(39):16470–80.

77. Berti L, Alessandrini A, Facci P. DNA-templated photoinduced silver deposition. J Am Chem Soc. 2005;127(32):11216–7.

78. Ruff LE, Sapre AA, Plaut JS, De Maere E, Mortier C, Nguyen V, et al. Selection of DNA nanoparticles with preferential binding to aggregated protein target. Nucleic Acids Res. 2016;44(10):1–11.

79. Med S, Tez S, Ke ZEM, Tibb LU, Anab MYA, Dani D, et al. Manyetik nanoparçaciklarin pankreas kanser hücre hattina özgü dna nanoparçaciklari ile modifikasyonu yoluyla hücreye hedeflendirilmesi. 2020;

80. Yoe JH, Jones AL. Colorimetric Determination of Iron with Disodium-1,2-dihydroxybenzene-3,5-disulfonate. Ind Eng Chem - Anal Ed. 1944;16(2):111–5.

81. Garaio E, Sandre O, Collantes JM, Garcia JA, Mornet S, Plazaola F. Specific absorption rate dependence on temperature in magnetic field hyperthermia measured by dynamic hysteresis losses (ac magnetometry). Nanotechnology. 2015;26(1).

82. Zhang J, Boyd C, Luo W. Two Mechanisms and a Scaling Relation for Dynamics in Ferrofluids. Phys Rev Lett. 1996;77(2):390–3.

83. Tompkins J, Huitink D. Induction heating response of iron oxide nanoparticles in varyingly viscous mediums with prediction of brownian heating contribution. Nanoscale Microscale Thermophys Eng [Internet]. 2020;00(00):1–15. Available from: https://doi.org/10.1080/15567265.2020.1806968

84. Zhang LY, Gu HC, Wang XM. Magnetite ferrofluid with high specific absorption

rate for application in hyperthermia. J Magn Magn Mater. 2007;311(1 SPEC. ISS.):228–33.